

Article

# Cobalt Based Catalysts Supported on Two Kinds of Beta Zeolite for Application in Fischer-Tropsch Synthesis

Renata Sadek <sup>1,2</sup>, Karolina A. Chalupka <sup>1</sup>, Pawel Mierczynski <sup>1</sup> , Jacek Rynkowski <sup>1,\*</sup>, Jacek Gurgul <sup>3</sup>  and Stanislaw Dzwigaj <sup>2,\*</sup>

<sup>1</sup> Lodz University of Technology, Institute of General and Ecological Chemistry, Zeromskiego 116, 90-924 Lodz, Poland; renata.sadek90@gmail.com (R.S.); karolina.chalupka@p.lodz.pl (K.A.C.); pawel.mierczynski@p.lodz.pl (P.M.)

<sup>2</sup> Laboratoire de Réactivité de Surface, Sorbonne Université-CNRS, UMR 7197, 4 Place Jussieu, Case 178, F-75252 Paris, France

<sup>3</sup> Jerzy Haber Institute of Catalysis and Surface Chemistry, Polish Academy of Sciences, Niezapominajek 8, PL 30239 Krakow, Poland; ncgurgul@cyf-kr.edu.pl

\* Correspondence: jacek.rynkowski@p.lodz.pl (J.R.); stanislaw.dzwigaj@upmc.fr (S.D.); Tel.: +48-426-313-125 (J.R.); +33-144-272-113 (S.D.)

Received: 9 May 2019; Accepted: 24 May 2019; Published: 29 May 2019



**Abstract:** Co-containing Beta zeolite catalysts prepared by a wet impregnation and two-step postsynthesis method were investigated. The activity of the catalysts was examined in Fischer-Tropsch synthesis (FTS), performed at 30 atm and 260 °C. The physicochemical properties of all systems were investigated by means of X-ray diffraction (XRD), in situ XRD, temperature programmed desorption of ammonia (NH<sub>3</sub>-TPD), X-ray Photoelectron Spectroscopy (XPS), temperature programmed reduction of hydrogen (TPR-H<sub>2</sub>), and transmission electron microscopy (TEM). Among the studied catalysts, the best results were obtained for the samples prepared by a two-step postsynthesis method, which achieved CO conversion of about 74%, and selectivity to liquid products of about 86%. The distribution of liquid products for Red-Me-Co<sub>20</sub>Beta was more diversified than for Red-Mi-Co<sub>20</sub>Beta. It was observed that significant influence of the zeolite dealumination of mesoporous zeolite on the catalytic performance in FTS. In contrast, for microporous catalysts, the dealumination did not play such a significant role and the relatively high activity is observed for both not dealuminated and dealuminated catalysts. The main liquid products of FTS on both mesoporous and microporous catalysts were C<sub>10</sub>-C<sub>14</sub> isoalkanes and n-alkanes. The iso-/n-alkanes ratio for dealuminated zeolite catalysts was three times higher than that for not dealuminated ones, and was related to the presence of different kind of acidic sites in both zeolite catalysts.

**Keywords:** cobalt; Beta; zeolites; Fischer-Tropsch synthesis

## 1. Introduction

The growing demand for high-quality energy puts new challenges for scientists in the field of alternative fuels production. For this reason, for many years a considerable interest has been focused on technology and catalysts for Fischer-Tropsch synthesis (FTS). This process leads to the production of sulfur and nitrogen free fuels and other valuable chemical compounds from the synthesis gas (the mixture of CO and H<sub>2</sub>). The most known catalysts of the Fischer-Tropsch reaction are metal oxides (Fe, Co, Ru, Ni), which are often supported on Al<sub>2</sub>O<sub>3</sub>, SiO<sub>2</sub>, mesoporous silica and zeolites [1–10]. Cobalt catalysts are more widely used in FTS, which is related to both their higher selectivity for paraffins

and low activity in a water gas shift reaction. Compared to iron catalysts, Co based systems are less susceptible to sintering and deactivation by carbon deposit [11].

The use of a suitable carrier plays a crucial role in the activity and selectivity of catalysts. This is due to the fact that the increase of the hydrocarbon chains in FTS occurs on the metallic cobalt nanoparticles. The type of the carrier used influence both the dispersion of active phase and the susceptibility to reduction of cobalt oxides. Strong metal-support interaction (SMSI) observed, for example, in Co/Al<sub>2</sub>O<sub>3</sub> can lead to the formation of the difficult to reduce cobalt species, and hence a reduction of the catalyst activity. In addition, the presence of the acidic site in the structure of the support results in the transformation of previously formed products into short-chain, saturated, and unsaturated hydrocarbons through cracking, aromatization, and isomerization processes [11]. According to Subramanian et al. [7], the application of the Co/SiO<sub>2</sub> in this synthesis leads to obtaining only a small fraction of isoparaffins, related to the absence of the strong acid sites on the carrier surface. Moreover, the present of strong acid sites in Co/H-ZSM-5 influence mainly the selectivity to the C<sub>5</sub>-C<sub>12</sub> hydrocarbons. The different phenomenon was observed in the case of long-chain hydrocarbons, where the greater role in hydrocracking and isomerization plays the steric effects [7]. The application of CoZSM-5 having in its structure weak acid sites exhibited greater selectivity to C<sub>5</sub>-C<sub>8</sub> hydrocarbons [12].

It is also worth noting, that the increase in the amount of acid sites, present in close proximity to the Co active sites, enhances the selectivity towards isoparaffins [13]. Xing et al. [14] noticed that too high a ratio of strong Brønsted to Lewis acid sites may cause overcracking of previously obtained products, leading to lower selectivity towards isoparaffins. Furthermore, the diminishing of the Si/Al ratio caused the increase of the deactivation rate. This phenomenon is related to carbon deposition on the catalyst surface, which blocks the access to active sites [15,16].

The nature and the state of cobalt particles also might have an influence on the Fischer-Tropsch synthesis. It has been reported by Concepción et al. [17] that the improvement of selectivity to C<sub>5+</sub> is connected with a higher concentration of coordinatively unsaturated Co<sup>0</sup> centers. Furthermore, the presence of unreduced cobalt oxide species leads to the increase of the activity of catalyst in water-gas shift reaction [18].

The aim of our work was to investigate the effect of dealumination of Beta zeolite and presence of mesopores in the zeolite matrix on the Fischer-Tropsch synthesis. For this purpose, the not dealuminated, partially and totally dealuminated Beta zeolite were prepared and used as supports for preparation of Co-containing Beta zeolite catalysts. As a support for these catalysts, two types of Beta zeolite were chosen with micro- and mesoporous structure. The used catalytic systems in FTS were the subject of extensive physicochemical characterization by XRD, in situ XRD, NH<sub>3</sub>-TPD, XPS, TPR-H<sub>2</sub>, TEM, and TG-DTA-MS.

## 2. Results and Discussion

### 2.1. Structural Properties

XRD patterns of the tested samples show two main reflections at 2θ close to 7.70 and 22.50° characteristic for the Beta zeolite (Figure 1). Their presence is most likely related to the co-existence of two isomorphous forms of Beta zeolite [19]. The removing of Al from the framework of Beta zeolite and introduction of 20% wt of Co do not affect crystallinity of zeolite, what is confirmed by similar XRD patterns. Based on our earlier studies, upon introduction of Co into the structure of Beta zeolite, the values of 2θ around 22.44° for Me-HAlBeta and Mi-HAlBeta, 22.54° for Me-HAlSiBeta, 22.66° for Me-SiBeta, 22.68° for Mi-HAlSiBeta and 22.78° for Mi-SiBeta (results not shown) decrease to 22.37° for Me-Co<sub>20</sub>AlBeta, to 22.43° for Me-Co<sub>20</sub>AlSiBeta and Mi-Co<sub>20</sub>AlBeta, to 22.47° for Me-Co<sub>20</sub>SiBeta and Mi-Co<sub>20</sub>AlSiBeta and to 22.57° for Mi-Co<sub>20</sub>SiBeta, respectively, indicating expansion of the zeolite framework [20,21]. The reflections at 2θ = 36.80, 59.30 and 65.20° correspond to the Co<sub>3</sub>O<sub>4</sub> oxide phase [16,17,22].

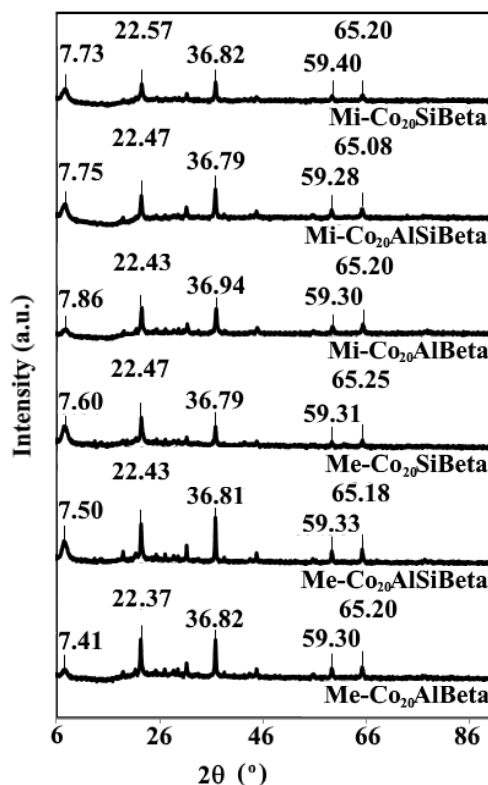


**Figure 1.** X-ray diffractograms measured at room temperature and ambient atmosphere of Me-Co<sub>20</sub>AlBeta, Me-Co<sub>20</sub>AlSiBeta, Me-Co<sub>20</sub>SiBeta, Mi-Co<sub>20</sub>AlBeta, Mi-Co<sub>20</sub>AlSiBeta and Mi-Co<sub>20</sub>SiBeta.

Figures 2 and 3 present XRD patterns of tested zeolite catalysts recorded in situ at 300 and 400 °C. It can be noticed that the two-step reduction of Co<sub>3</sub>O<sub>4</sub> takes place at 300 °C. In the first step, the formation of CoO is detected (reflexes at 2θ around 42.30° and 61.23°), followed by the partial reduction to Co<sup>0</sup> (2θ around 44.20°). For the sample reduced at 400 °C the reflection related to metallic cobalt (at 2θ around 44.15°) predominates, however a small reflection around 42.30° associated to CoO is still visible [23–25]. It shows that the oxide phase is not completely reduced at 400 °C.

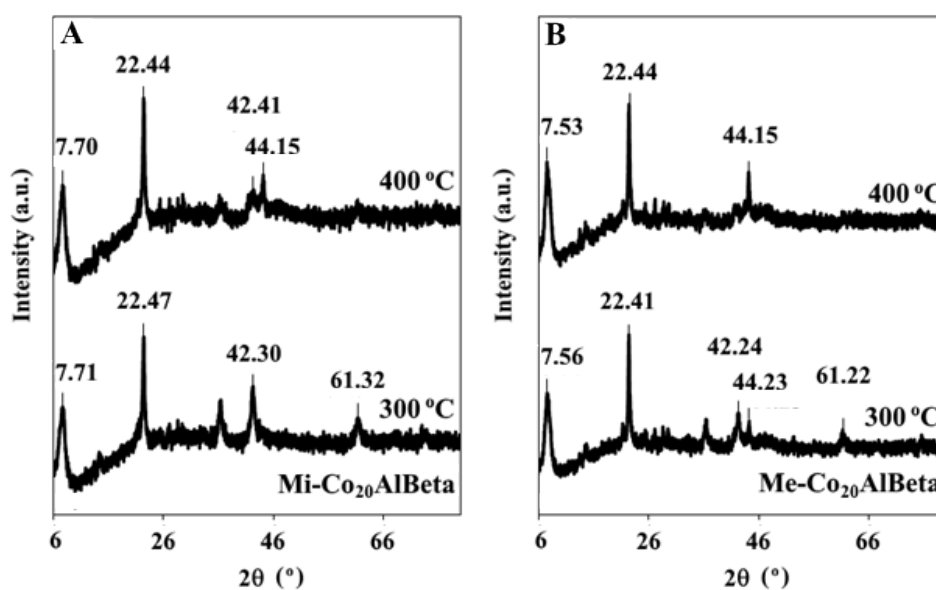


**Figure 2.** In situ XRD patterns recorded in situ at 300 and 400 °C measured in the atmosphere of the mixture of 5 vol % hydrogen in argon (A) Mi-Co<sub>20</sub>AlBeta and (B) Me-Co<sub>20</sub>AlBeta.

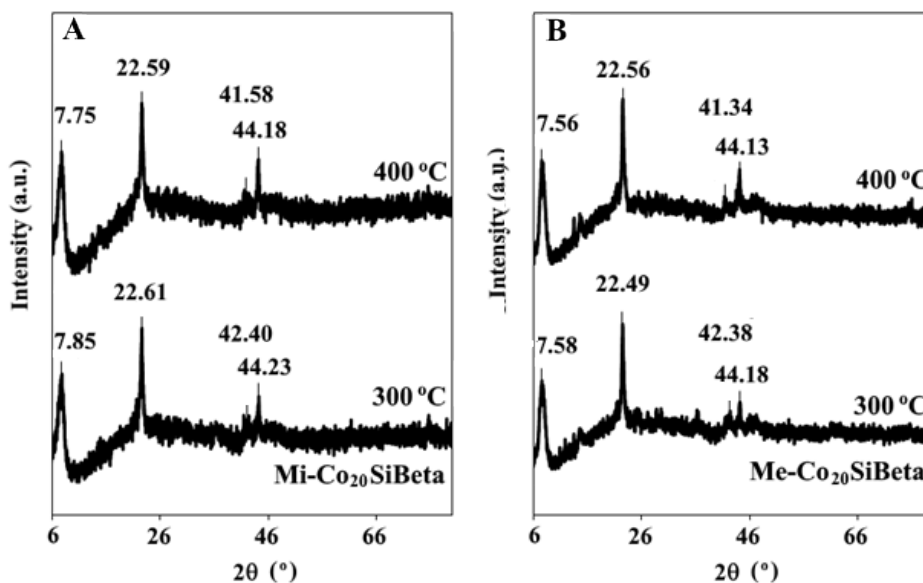


**Figure 3.** In situ XRD patterns recorded in situ at 300 and 400 °C measured in the atmosphere of the mixture of 5 vol % hydrogen in argon (A) Mi-Co<sub>20</sub>SiBeta and (B) Me-Co<sub>20</sub>SiBeta.

## 2.2. Characterisation of Zeolite Catalysts by XPS

The X-ray photoelectron spectra of microporous and mesoporous Co-containing Beta zeolites have been analysed numerically in the BE regions of Si 2p, Al 2p, O 1s, C 1s and Co 2p.

All Si 2p spectra are well fitted by three doublets with the spin-orbit splitting of 0.61 eV (not shown here). Relative intensities of these components do not depend on the porosity of zeolite matrix. The most intense components (>94%) with Si 2p<sub>3/2</sub> BE values of 103.8–104.3 eV can be identified as tetrahedral Si(IV) species [26–31]. It is worth mentioning here that these values are slightly larger than reported recently for MOR, BEA and MFI zeolites elsewhere [32]. There is a visible increase of area of low-BE component (Si 2p<sub>3/2</sub> BE of 101.4–101.9 eV) in AlBeta samples. Such low-BE is characteristic for silicon in lower than 4+ oxidation state and can be associated to Si present in Si-O(H)-Al groups. Moreover, in AlSiBeta samples one can find that high-BE components are significantly larger than in other samples. Above mentioned facts point out that the dealumination process can influence the silicon environment.

The O 1s peaks can be well described by three components: (i) a main peak located at 533.3–533.7 eV related to oxygen in the zeolite framework [33,34]; (ii) a much smaller peak at 531.0–531.4 eV assigned to oxygen–metal bonds; (iii) a peak at BE higher than 534 eV due to OH groups, adsorbed water and/or oxygen of organic contaminants. There are some differences between intensities of individual components in AlBeta and AlSiBeta samples with micro- and mesoporous structures, in contrast to both SiBeta samples, which are almost the same.

The C 1s core lines consist of three peaks at 285.0 eV (organic contaminants), 286.0–286.2 eV (C–O groups) and >289 eV (C=O groups). In case of AlSiBeta high-BE components have slightly lower binding energies of 288.1–288.4 eV.

The binding energy of all Al 2p<sub>3/2</sub> peaks is close to 75.3 eV indicating the presence in all Beta zeolite materials of Al<sup>3+</sup> (Al<sub>2</sub>O<sub>3</sub> BE = 74.9 eV).

Figures 4 and 5 presents Co 2p XP spectra of microporous and mesoporous CoBeta zeolites, respectively. Co 2p core lines are splitted into well-separated spin-orbit doublet structures (Co 2p<sub>3/2</sub> and 2p<sub>1/2</sub>) coming from the charge-transfer (CT) states 2p<sup>5</sup>3d<sup>8</sup>L<sup>-1</sup> (L - ligand). Respective satellite maxima, which overlap the main lines, reflect non-CT 2p<sup>5</sup>3d<sup>7</sup> states. The main parameters of the fitted components are presented in Table 1. The spin-orbit splitting of Co 2p doublets in the range of 15.4–16.8 eV and the occurrence of strong satellites are characteristic of the high-spin cobalt(II). Except Mi-Co<sub>20</sub>SiBeta, all spectra have to be fitted with at least two doublets and associated satellites. For

simplicity, and taking into account that both components are related to Co(II) species, only one satellite line is used but with a broadened FWHM.

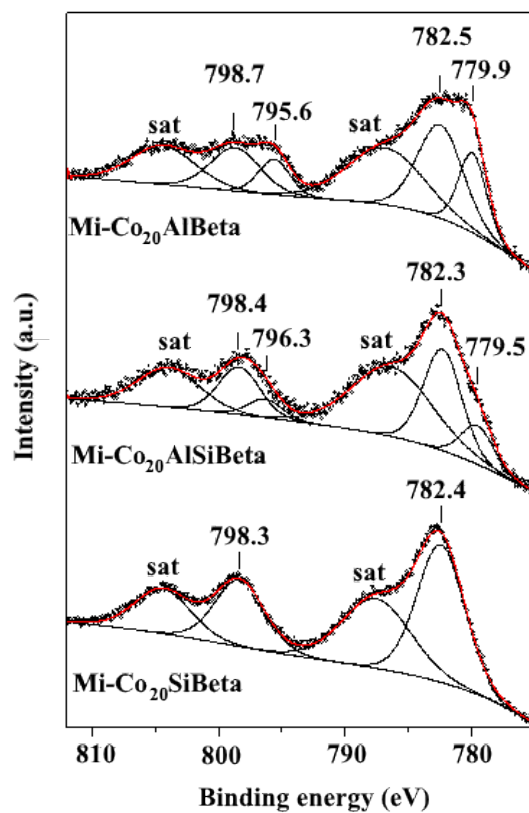


Figure 4. Co 2p photoelectron spectra of microporous  $\text{Co}_{20}\text{Beta}$  zeolites.

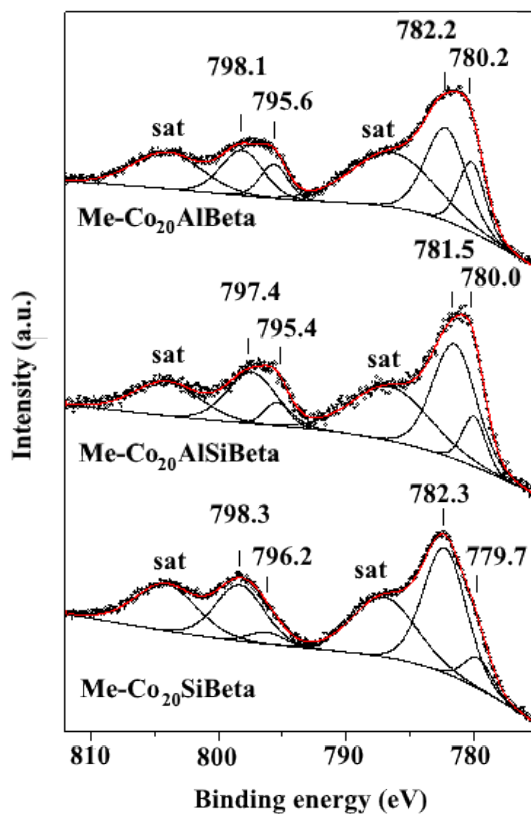


Figure 5. Co 2p photoelectron spectra of mesoporous  $\text{Co}_{20}\text{Beta}$  zeolites.

**Table 1.** The BE values (eV) and relative areas of components (%) of Co 2p core excitations obtained for microporous Mi-Co<sub>20</sub>Beta and mesoporous Me-Co<sub>20</sub>Beta zeolites.

Zeolites	A	A'	B	B'	Satellite	Satellite
Me-Co <sub>20</sub> AlBeta	780.2 (29.5)	795.6	782.3 (70.5)	798.0	787.1	804.0
Mi-Co <sub>20</sub> AlBeta	779.9 (34.2)	795.6	782.5 (65.8)	798.7	786.8	804.4
Me-Co <sub>20</sub> AlSiBeta	780.0 (31.1)	795.4	781.8 (68.9)	797.6	786.4	803.9
Mi-Co <sub>20</sub> AlSiBeta	779.5 (24.4)	796.3	782.3 (75.6)	798.4	786.3	803.9
Me-Co <sub>20</sub> SiBeta	779.7 (16.1)	796.2	782.3 (83.9)	798.3	786.9	804.1
Mi-Co <sub>20</sub> SiBeta	—	—	782.4 (100)	798.5	787.7	804.5

For Co-containing Beta zeolites under study, all low-BE Co 2p<sub>3/2</sub> components have values in the range of 779.5–780.2 eV. Bear in mind, that BE of Co 2p<sub>3/2</sub> peak is revealed to be 780.0–780.9 eV for CoO, 779.4–780.1 eV for Co<sub>3</sub>O<sub>4</sub> and 780.0–780.3 eV for Co(OH)O [35], one can identify this component as coming from an extra-framework oxide. The dominant component with BE values in the range of 781.8–782.5 eV comes from Co(II) species incorporated into the zeolite matrix. Such high BE values of Co species were observed for CoBeta (782.6 eV) [36], washcoated CoFerrierite and Co<sup>2+</sup>-exchanged NaY (782.7–782.9 eV) [37,38] and for highly dispersed Co species in Co-ZSM-5 [39] (783.2 eV) with cobalt coordinated to lattice oxygen and probably incorporated into vacant T-atom sites [40]. It is well known that many metal cations located in zeolites also show higher BE comparing with their BE in oxides [41–43], which can be related to the degree of cations dispersion as well as the type of their interactions with the zeolite matrix in which they are incorporated.

The relative intensities of low-BE components are significantly decreased after the dealumination process, which is especially well visible in case of microporous samples (Figure 4). There is no low-BE component in Mi-SiBeta at all, whereas in Mi-AlBeta it covers over 30% of total spectrum area. Moreover, there is a visibly shift of this component to higher BE suggesting that the Co<sup>3+</sup>/Co<sup>2+</sup> molar ratio of oxide species (CoO and Co<sub>3</sub>O<sub>4</sub>) can change (see Figure 5), which is in line with XRD results.

### 2.3. Characterisation of Acidity by NH<sub>3</sub>-TPD

The acidity of the catalysts was determined by NH<sub>3</sub>-TPD method. One can observe peaks in the temperature ranges 124–210°C and 395–489°C, which are related to weak and strong acidic sites, respectively (Figure 6) [13,16,44]. The elimination of strong acidic sites during the dealumination procedure causes a shift of high-temperature peak to lower temperature, as stated by earlier work [16]. Contrary to the Mi-Co<sub>20</sub>AlSiBeta, Me-Co<sub>20</sub>AlSiBeta and Mi-Co<sub>20</sub>SiBeta, the reduction of Me-Co<sub>20</sub>SiBeta and not dealuminated samples caused an increase in the high-temperature peak intensity.

The highest acidity of the Co-containing dealuminated zeolites is associated to the formation of Co(II) Lewis acidic sites (Table 2). The Me-Co<sub>20</sub>AlSiBeta and Mi-Co<sub>20</sub>AlSiBeta present the smallest amount of adsorbed NH<sub>3</sub>. It is related to the blockage of the pores by cobalt oxides and removal of strong acidic sites [16].

Furthermore, the reduction of Mi-Co<sub>20</sub>AlBeta and Me-Co<sub>20</sub>AlBeta increased the number of acidic sites. This phenomenon is probably caused by reappearance of Lewis and/or Brønsted acidic sites. However, in case of Red-Co<sub>20</sub>AlSiBeta and Red-Co<sub>20</sub>SiBeta, the decrease of the amount of adsorbed NH<sub>3</sub> is observed, which may be related to both form the reduction of Co (II) Lewis acidic sites as well as the creation of nanoparticles of Co.

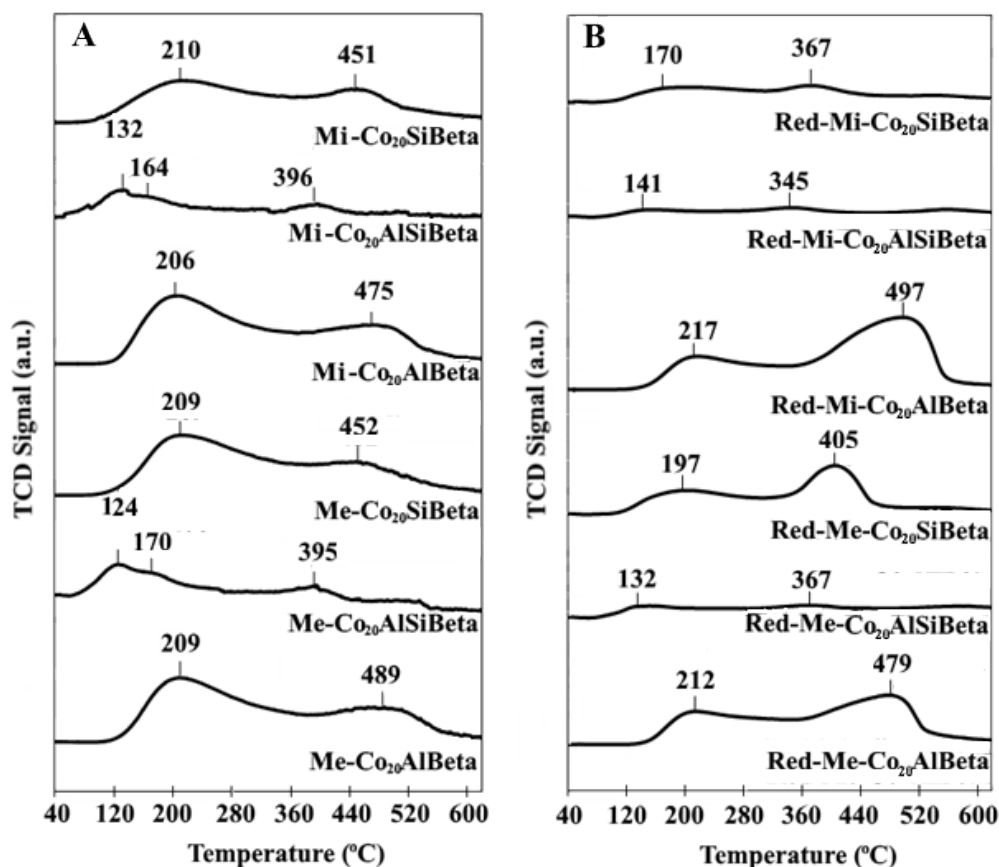


**Figure 6.** NH<sub>3</sub>-TPD profiles of (A) Me-Co<sub>20</sub>AlBeta, Me-Co<sub>20</sub>AlSiBeta, Me-Co<sub>20</sub>SiBeta, Mi-Co<sub>20</sub>AlBeta, Mi-Co<sub>20</sub>AlSiBeta and Mi-Co<sub>20</sub>SiBeta and (B) Red-Me-Co<sub>20</sub>AlBeta, Red-Me-Co<sub>20</sub>AlSiBeta, Red-Me-Co<sub>20</sub>SiBeta, Red-Mi-Co<sub>20</sub>AlBeta, Red-Mi-Co<sub>20</sub>AlSiBeta and Red-Mi-Co<sub>20</sub>SiBeta.

#### 2.4. Reducibility of CoSiBeta Catalysts

TPR profiles of microporous Mi-Co<sub>20</sub>Beta and mesoporous Me-Co<sub>20</sub>Beta zeolites are presented in Figure 7. Hydrogen consumption in the temperature range ca. 300–630 °C indicates the presence of extra framework cobalt oxides [45]. The occurrence of two maxima, the first one at 369–414 °C and the second one at 401–485 °C suggests two-step reduction of Co<sub>3</sub>O<sub>4</sub> (Co<sub>3</sub>O<sub>4</sub> → CoO → Co<sup>0</sup>) [10,16].

For totally dealuminated catalysts, Mi-Co<sub>20</sub>SiBEA and Me-Co<sub>20</sub>SiBEA, the additional peak with maximum at 840–869 °C is observed. It may be associated with the reduction of pseudo-tetrahedral Co(II) present in the framework of Beta zeolite [45]. No significant differences between the reducibility of cobalt species in both types of microporous (Mi) and mesoporous (Me) Beta zeolite catalysts are observed.

#### 2.5. Characterisation of Cobalt Nanoparticles by TEM

The distribution and average crystallite size of the cobalt nanoparticles formed in all microporous Red-Mi-Co<sub>20</sub>Beta and mesoporous Red-Me-Co<sub>20</sub>Beta zeolites are presented in Figures 8–10 and Table 2. The average size of the cobalt nanoparticles in Red-Me-Co<sub>20</sub>AlBeta (80.0 nm), Red-Me-Co<sub>20</sub>AlSiBeta (68.3 nm), and Red-Me-Co<sub>20</sub>SiBeta (37.2 nm) is bigger than in Red-Mi-Co<sub>20</sub>AlBeta (51.9 nm), Red-Mi-Co<sub>20</sub>AlSiBeta (45.0 nm) and Red-Mi-Co<sub>20</sub>SiBeta (34.1 nm), respectively. The presence of mesopores in the zeolite structure leads to the formation of larger Co particles. The similar phenomenon was observed by Khodakov et al. [4] for MCM-41 and SBA-15. Furthermore, mesoporous samples exhibit less diversified metal nanoparticles distribution than the microporous ones. For Red-Me-Co<sub>20</sub>Beta zeolites the significant contribution (40–50%) of cobalt nanoparticles bigger than 50 nm is observed.

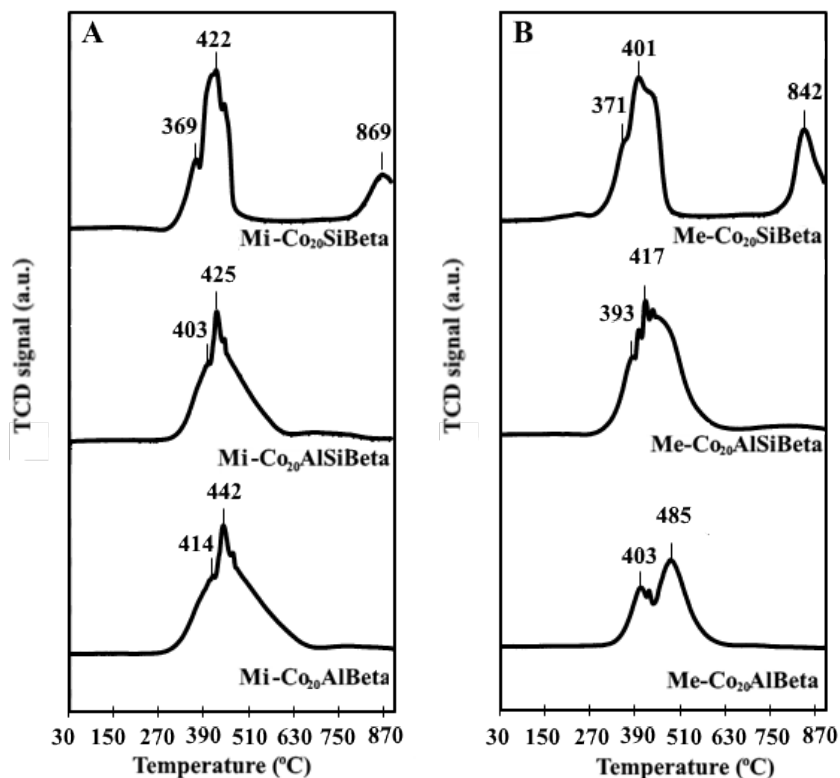


Figure 7. TPR-H<sub>2</sub> profiles of microporous Mi-Co<sub>20</sub>Beta (A) and mesoporous Me-Co<sub>20</sub>Beta zeolites (B).

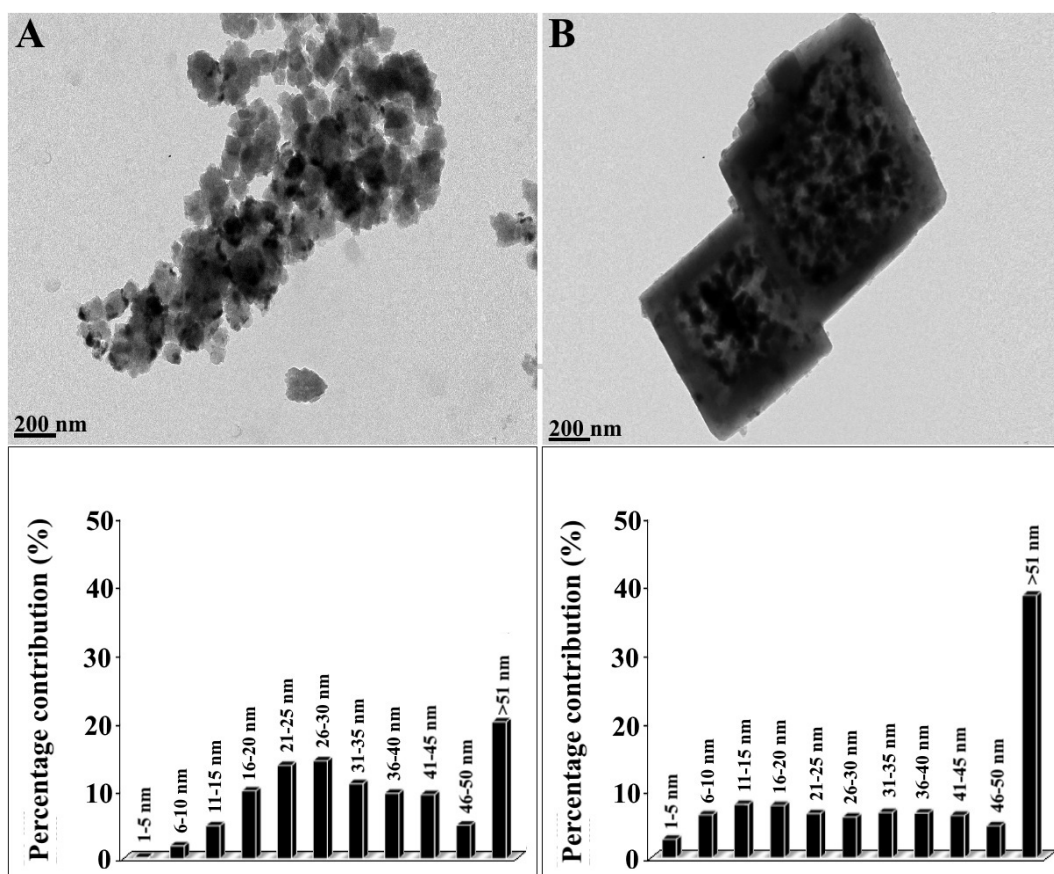
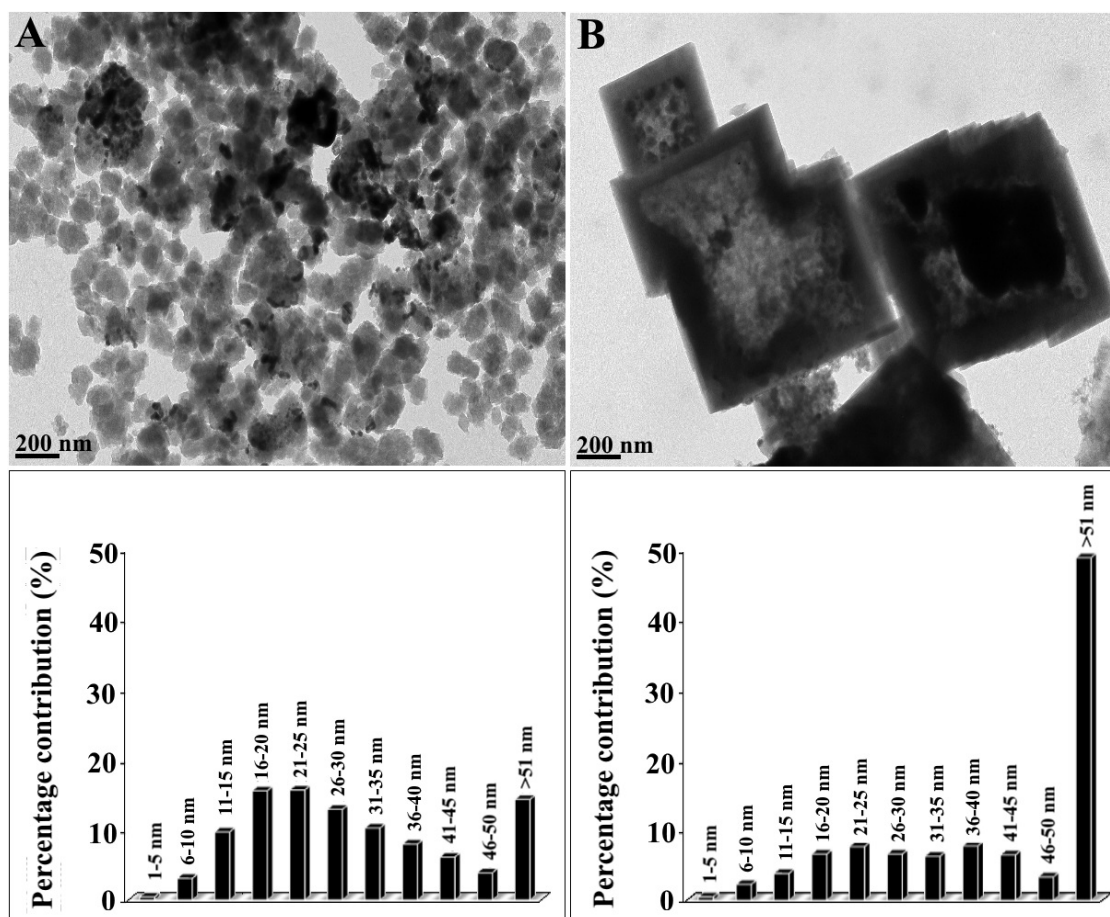
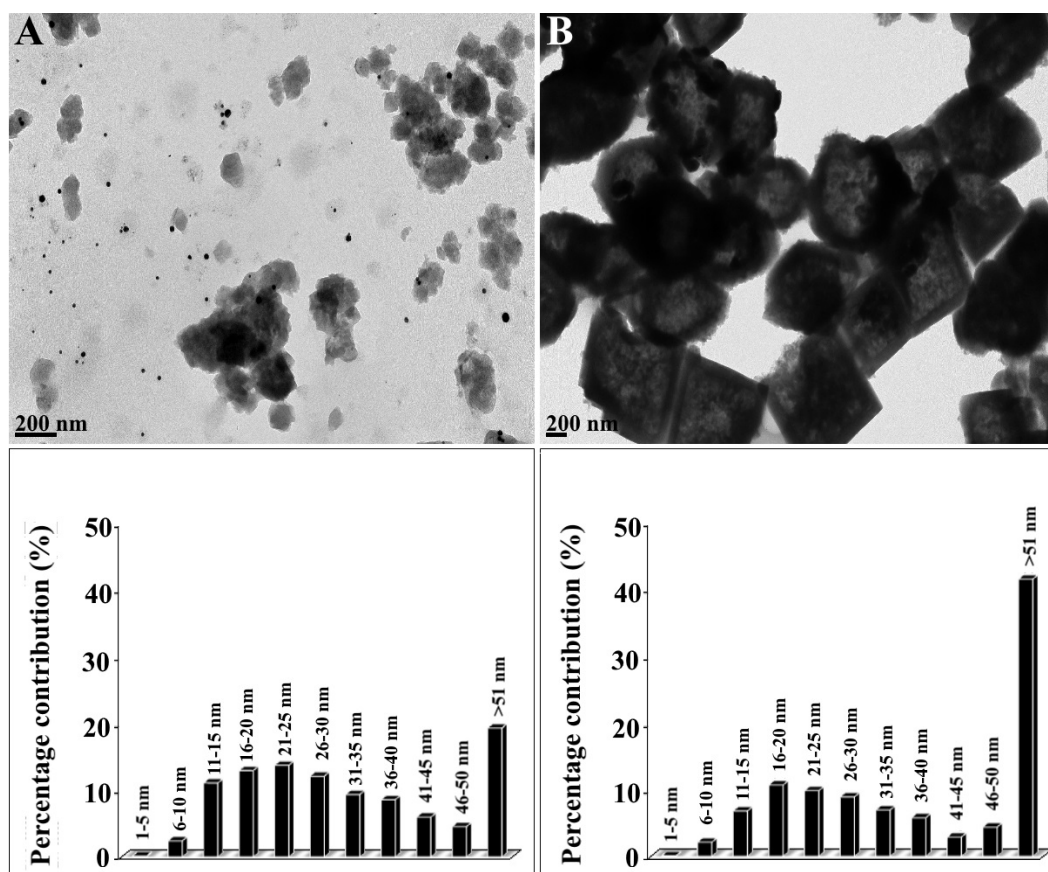


Figure 8. TEM images and metal nanoparticle size distribution on (A) Red-Mi-Co<sub>20</sub>AlBeta and (B) Red-Me-Co<sub>20</sub>AlBeta.

**Table 2.** The average crystallites size and amount of NH<sub>3</sub> adsorbed on Co-containing Beta zeolites.

Sample	NH <sub>3</sub> [ $\mu\text{mol/g}$ ]	Average Crystallites Size [nm]
Me-Co <sub>20</sub> SiBeta	1202	
Red-Me-Co <sub>20</sub> SiBeta	1178	80.0
Me-Co <sub>20</sub> AlSiBeta	522	
Red-Me-Co <sub>20</sub> AlSiBeta	301	68.3
Me-Co <sub>20</sub> AlBeta	1316	
Red-Me-Co <sub>20</sub> AlBeta	1741	37.2
Mi-Co <sub>20</sub> SiBeta	915	
Red-Mi-Co <sub>20</sub> SiBeta	647	51.9
Mi-Co <sub>20</sub> AlSiBeta	253	
Red-Mi-Co <sub>20</sub> AlSiBeta	220	45.0
Mi-Co <sub>20</sub> AlBeta	1442	
Red-Mi-Co <sub>20</sub> AlBeta	2279	34.1

**Figure 9.** TEM images and metal nanoparticle size distribution on (A) Red-Mi-Co<sub>20</sub>AlSiBeta and (B) Red-Me-Co<sub>20</sub>AlSiBeta.



**Figure 10.** TEM images and metal nanoparticle size distribution on (A) Red-Mi-Co<sub>20</sub>SiBeta and (B) Red-Me-Co<sub>20</sub>SiBeta.

## 2.6. Catalytic Activity in Fischer-Tropsch Synthesis

The Red-Me-Co<sub>20</sub>Beta and Red-Mi-Co<sub>20</sub>Beta zeolite catalysts were tested in Fischer–Tropsch synthesis. The CO conversion and selectivity towards gaseous hydrocarbons, CO<sub>2</sub> and liquid products are presented in Figures 11–13 and Table 3. In the first several hours of the catalytic test, the CO conversion for all catalysts under study was low. After about 15 h of activation in the reaction conditions, the conversion has stabilized on the maximum level. In the following hours the more or less decrease in catalysts activity was observed. In Figures 11–13, the data from 15 to 20 hrs of reaction course is shown. For comparison of the catalysts performance some data after 20 hrs is presented in Table 3.

**Table 3.** The catalytic performance of tested samples after 20 h of reaction.

Catalysts	CO Conversion [Mole%]	Selectivity Towards C <sub>1</sub> -C <sub>4</sub> and CO <sub>2</sub> [Mole%]	Selectivity towards Liquid Products [Mole%]	iso/n-Alkane Ratio	Alcohols/n-Alkane Ratio	Unsaturated/n-Alkane Ratio	α C <sub>5+</sub>
Red-Mi-Co <sub>20</sub> AlBeta	70.81	18.30	81.70	2.21	-	0.54	0.76
Red-Mi-Co <sub>20</sub> AlSiBeta	40.85	17.08	82.92				
Red-Mi-Co <sub>20</sub> SiBeta	98.97	18.61	81.39				
Red-Me-Co <sub>20</sub> AlBeta	7.12	31.74	68.26	1.79	-	0.45	0.91
Red-Me-Co <sub>20</sub> AlSiBeta	48.52	9.44	87.56				
Red-Me-Co <sub>20</sub> SiBeta	99.56	18.27	81.74	1.48	0.21	0.46	0.63

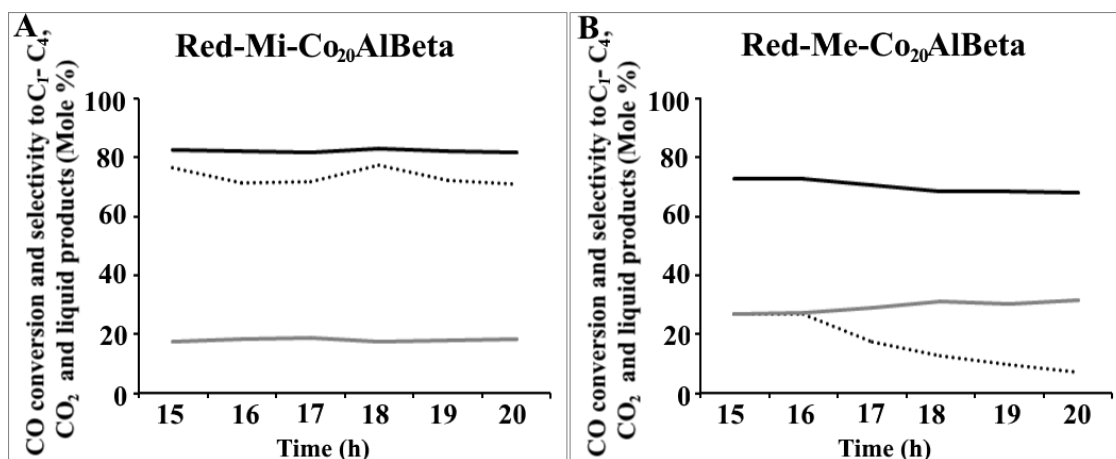


Figure 11. The conversion of CO (•••) and selectivity towards C<sub>1</sub>-C<sub>4</sub> (—) and liquid products (—) up to 20 h of reaction at 260°C and 30 atm on (A) Red-Mi-Co<sub>20</sub>AlBeta and (B) Red-Me-Co<sub>20</sub>AlBeta.

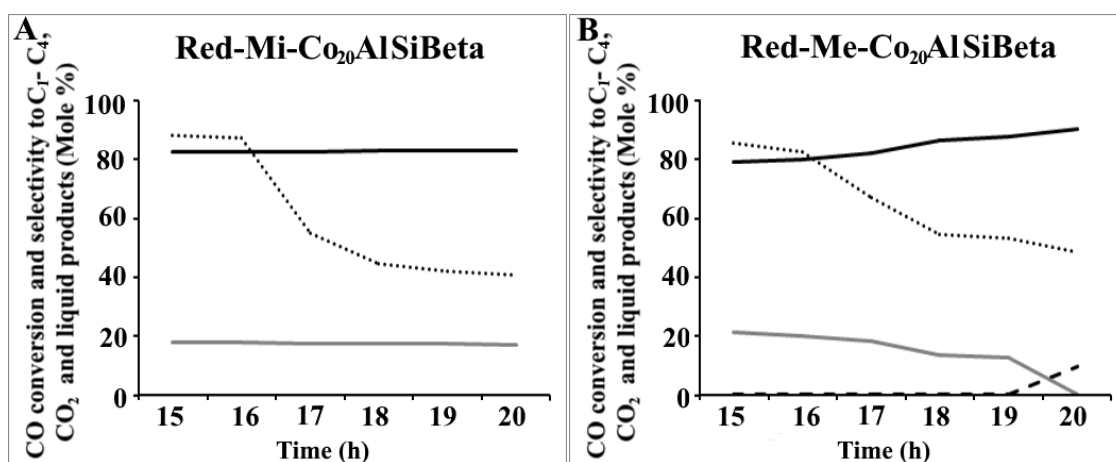


Figure 12. The conversion of CO (•••) and selectivity towards C<sub>1</sub>-C<sub>4</sub> (—), CO<sub>2</sub> (—) and liquid products (—) up to 20 h of reaction at 260 °C and 30 atm on (A) Red-Mi-Co<sub>20</sub>AlSiBeta and (B) Red-Me-Co<sub>20</sub>AlSiBeta.

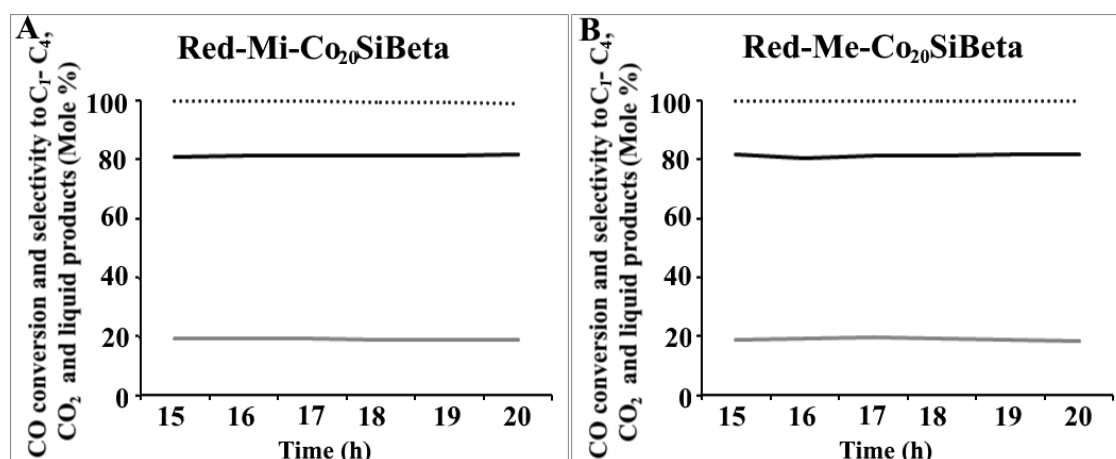


Figure 13. The conversion of CO (•••) and selectivity towards C<sub>1</sub>-C<sub>4</sub> (—) and liquid products (—) up to 20 h of reaction at 260°C and 30 atm on (A) Red-Mi-Co<sub>20</sub>SiBeta and (B) Red-Me-Co<sub>20</sub>SiBeta.

In the case of mesoporous zeolite catalysts, the increase of CO conversion with increasing of the dealumination degree was observed (from 7% for Red-Co<sub>20</sub>AlBeta to 99.6% for Red-Co<sub>20</sub>SiBeta).

Moreover, it seems that the increase of nanoparticles size leads to the improvement of catalytic activity of Red-Me-Co<sub>20</sub>Beta catalysts. It was noticed that in the case of not dealuminated sample–Red-Me-Co<sub>20</sub>AlBeta, the average size of nanoparticles is 37 nm, while for partially (Red-Me-Co<sub>20</sub>AlSiBeta) and completely dealuminated (Red-Me-Co<sub>20</sub>SiBeta) zeolite catalysts the average size of cobalt particles is 68 and 80 nm, respectively.

It is worth mentioning that catalytic behaviour of Red-Mi-Co<sub>20</sub>SiBeta catalyst is very similar to the mesoporous zeolite catalysts (Red-Me-Co<sub>20</sub>SiBeta) and the changes in CO conversion and selectivity towards liquid hydrocarbons are the same as for mesoporous catalyst. However, the catalytic behaviour of non-dealuminated catalysts is entirely different and depends on the sample porosity, despite the fact that cobalt nanoparticles size in these samples is almost the same. As in the case of mesoporous catalysts, we also found the cobalt nanoparticles size increasing with the increase of dealumination degree (from 34 nm for non-dealuminated catalyst to 52 nm for completely dealuminated one).

The highest activity and selectivity towards liquid products are observed for dealuminated Red-Me-Co<sub>20</sub>SiBeta and Red-Mi-Co<sub>20</sub>SiBeta zeolite catalysts obtained by two-step postsynthesis method. The CO conversion of 99–99.6% and selectivity towards liquid products of 81–82% for these catalysts are achieved. The catalytic activity of these zeolite catalysts is stable throughout the duration of the reaction.

The catalytic activity of microporous non-dealuminated catalyst (Red-Mi-Co<sub>20</sub>AlBeta) is also on the high level and exhibits the CO conversion of 71% and selectivity towards liquid products near 82% (Figs. 11 and 13, Table 3). However, for partially dealuminated catalyst–Red-Mi-Co<sub>20</sub>AlSiBeta the significant decrease of catalytic activity is observed. This sample shows the CO conversion of 41% and selectivity towards liquid hydrocarbons of 83%. It should be noted that for the microporous Red-Mi-Co<sub>20</sub>AlBeta catalyst any important changes in CO conversion and selectivity towards liquid hydrocarbons are detected and this catalyst is very stable for all the time of the reaction course as opposed to not dealuminated mesoporous catalyst Red-Me-Co<sub>20</sub>AlBeta.

For Red-Mi-Co<sub>20</sub>Beta and Red-Mi-Co<sub>20</sub>SiBeta, the selectivity of about 17–18.6% towards C<sub>1</sub>–C<sub>4</sub> hydrocarbons is observed for 20 h of reaction. However, in case of Red- Co<sub>20</sub>AlBeta we noted the highest selectivity to C<sub>1</sub>–C<sub>4</sub> hydrocarbons equals 31.7%. It is also worth noting that only in the case of Red-Me-Co<sub>20</sub>AlSiBeta after 20 h of reaction we observed a decrease in the selectivity towards C<sub>1</sub>–C<sub>4</sub> from 12.4% to almost zero. Other authors observed a similar tendency during long-term synthesis as reported in [46,47]. Furthermore, after 19 h, the mesoporous partially dealuminated catalyst exhibited the selectivity to CO<sub>2</sub> of 9%. The carbon balance for gaseous products is presented in Table 4.

**Table 4.** Carbon balance for gaseous products (Carbon outlet = 0000821 mol min<sup>−1</sup>).

Sample	Reaction Time (h)	C <sub>1</sub> (n <sub>C</sub> =1n <sub>C1</sub> )	C <sub>2</sub> (n <sub>C</sub> =2n <sub>C2</sub> )	C <sub>3</sub> (n <sub>C</sub> =3n <sub>C3</sub> )	C <sub>4</sub> (n <sub>C</sub> =4n <sub>C4</sub> )	CO <sub>2</sub>	CO Outlet	Total outlet
Red-Mi-Co <sub>20</sub> AlBeta	15	0.00012	0.000034	0.000012	0.0000093	0	0.00018	0.00035
	20	0.000034	0.000202	0.000039	0.000009	0	0.000240	0.00052
Red-Me-Co <sub>20</sub> AlBeta	15	0.000090	0.00016	0.000014	0.0000068	0	0.00047	0.00074
	20	0.000093	0.000324	0.000007	0.000014	0	0.000793	0.00120
Red-Me-Co <sub>20</sub> SiBeta	15	0.000080	0.00015	0.0000039	0.0000035	0	0.0000025	0.00024
	20	0.000070	0.000157	0.000002	0.000004	0	0.000004	0.00024

The liquid products were analysed using gas chromatography coupled with mass spectrometry (GC–MS). Some results are shown in the Figure 14, whereas the quantitative analysis is shown in Table 3. In FT reaction performed on mesoporous Red-Me-Co<sub>20</sub>AlBeta and Red-Me-Co<sub>20</sub>SiBeta catalysts the main liquid products are isoalkanes and saturated hydrocarbons (C<sub>10</sub>–C<sub>14</sub>). The ratio of isoalkanes to n-alkanes is 1.8 for Red-Me-Co<sub>20</sub>AlBeta and 1.5 for Red-Me-Co<sub>20</sub>SiBeta (Figure 14B,C). In the case of FT reaction performed on microporous CoBeta catalysts isoalkanes and n-alkanes (C<sub>10</sub>–C<sub>14</sub>) are also identified. For Red-Mi-Co<sub>20</sub>AlBeta the isoalkanes to n-alkanes ratio is 2.2 (Figure 14 A). The iso-/n-alkanes ratio reached on cobalt Beta zeolite catalysts is unexpectedly high. It distinguishes

these zeolite catalysts from usually tested supported catalysts for which mainly the formation of linear hydrocarbons was observed. Satripi et al. [48] have noticed that cobalt supported catalysts—Co/SiO<sub>2</sub> and Co/HZSM-5 give very different products spectra at similar conversion levels. They have observed that gasoline range hydrocarbons are produced, and formation of waxes is eliminated in the case of Co/HZSM-5 catalyst, what means more amount of isoalkanes formation for these type of catalysts. Similar to Satripi et al. [44,48] we have also observed very high selectivity to gasoline-range products. They connect this high selectivity towards gasoline range hydrocarbons with “vicinity of the FT active phase to the acid functionality” [48]. Such a statement indicates that hydrocarbons chain propagation occurs on cobalt nanoparticles—active centres in Fischer-Tropsch synthesis and the cracking and isomerization of formed hydrocarbons takes place on acidic sites localized in zeolite matrix. It needs to underline that acidity of studied catalysts in this work is different and TPD profiles indicate a presence of various kind of acidic sites.

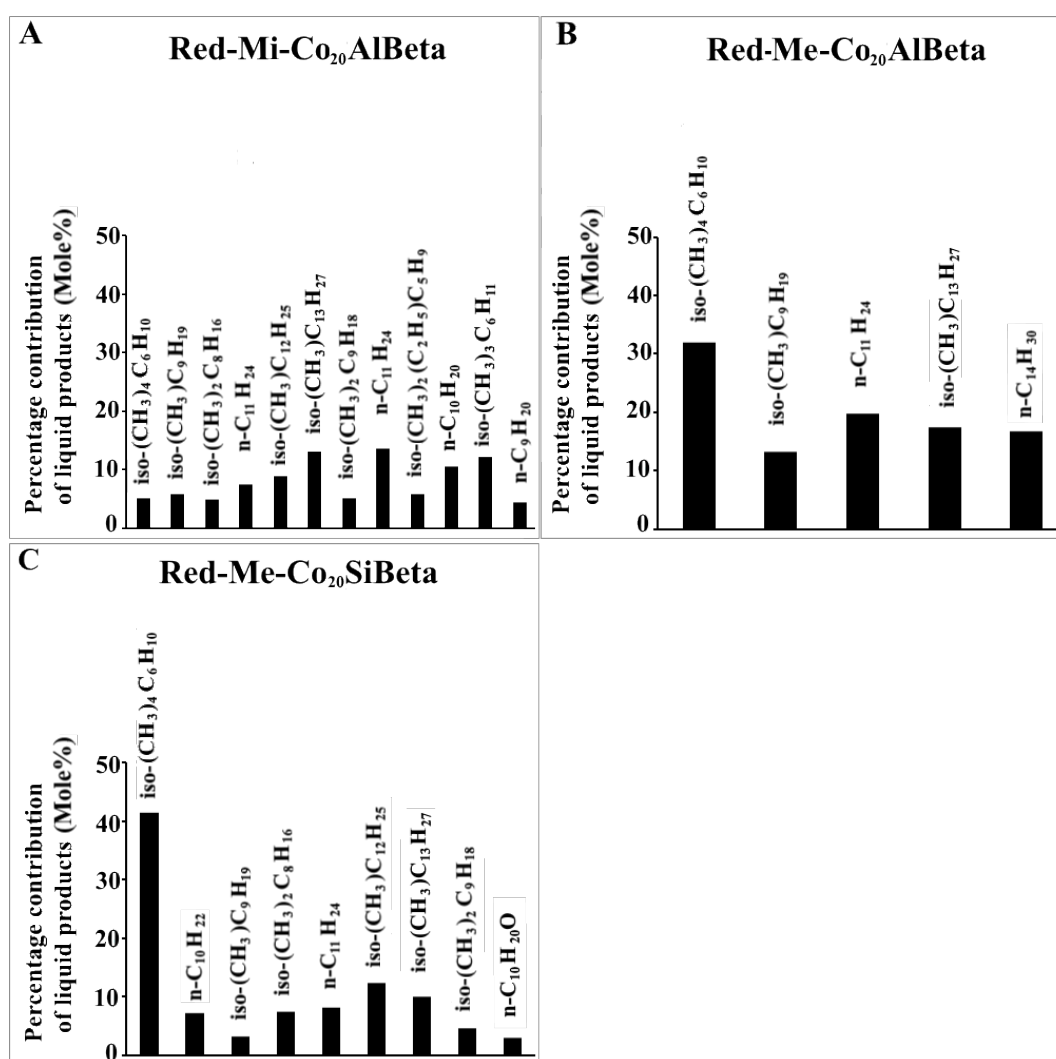


**Figure 14.** Distribution of compounds in liquid products obtained in FTS over (A) Red-Mi-Co<sub>20</sub>AlBeta, (B) Red-Me-Co<sub>20</sub>AlBeta and (C) Red-Me-Co<sub>20</sub>SiBeta.

Moreover, the very small amount of alcohols is identified only in the case of dealuminated sample (Red-Me-Co<sub>20</sub>SiBeta - 0.21). The similar observation was stated by Martinez and Lopez [49], who found that conversion of oxygenates to hydrocarbons was less pronounced for dealuminated samples containing a low amount of Brönsted acidic sites. For all systems, the formation of unsaturated hydrocarbons is noticed, and the ratio of them to n-alkanes is 0.54, 0.45 and 0.46 for Red-Mi-Co<sub>20</sub>AlBeta,

Red-Me-Co<sub>20</sub>AlBeta and Red-Me-Co<sub>20</sub>SiBeta, respectively. In order to determinate the value of chain growth probability ( $\alpha$ ) of obtained hydrocarbons Anderson–Schultz–Floury distribution is made. The  $\alpha$  value of Red-Mi-Co<sub>20</sub>AlBeta, Red-Me-Co<sub>20</sub>AlBeta and Red-Me-Co<sub>20</sub>SiBeta are 0.76, 0.91 and 0.63, respectively.

The significant problem in Fischer–Tropsch synthesis is carbon deposition, which cuts off the active sites of the reaction. We have investigated the type of carbon deposit by TG–DTA–MS technique. The results are presented in Figures 15–17. The oxidation of carbon takes place in several stages, what suggests the presence of different kinds of carbon species, relatively hard to oxidise. The oxidation proceeds up to 820 °C. The first (at c.a. 250 °C) and the second (at c.a. 400 °C) peaks are related to the removal of carbide species or waxes and polymeric carbon, which may be present on the support’s surface, respectively [16,50,51]. Additionally, one can see a high temperature peak at c.a. 840 °C for Spent-Red-Me-Co<sub>20</sub>AlBeta and Spent-Red-Mi-Co<sub>20</sub>AlSiBeta and Spent-Red-Me-Co<sub>20</sub>AlSiBeta and at c.a. 700 °C for Spent-Red-Mi-Co<sub>20</sub>SiBeta and Spent-Red-Me-Co<sub>20</sub>SiBeta), which can be associated with the removal of hard to oxidise graphitic carbon forms [51,52]. It is worth emphasizing that the temperature of carbon deposition removal decreases with the dealumination degree, what indicates that the dealumination process improves the resistance to carbon deposition.

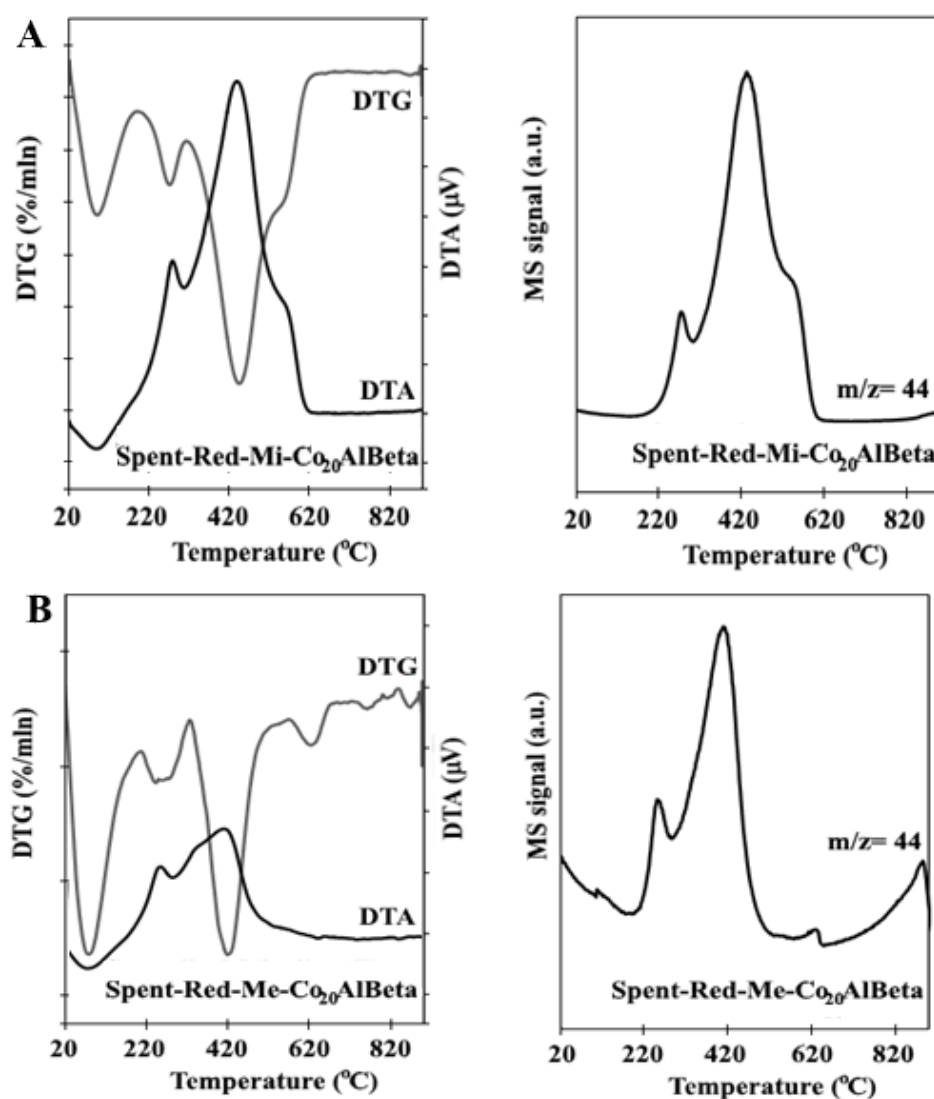


**Figure 15.** Investigation of carbon deposition on the (A) Spent-Red-Mi-Co<sub>20</sub>AlBeta and (B) Spent-Red-Me-Co<sub>20</sub>AlBeta.

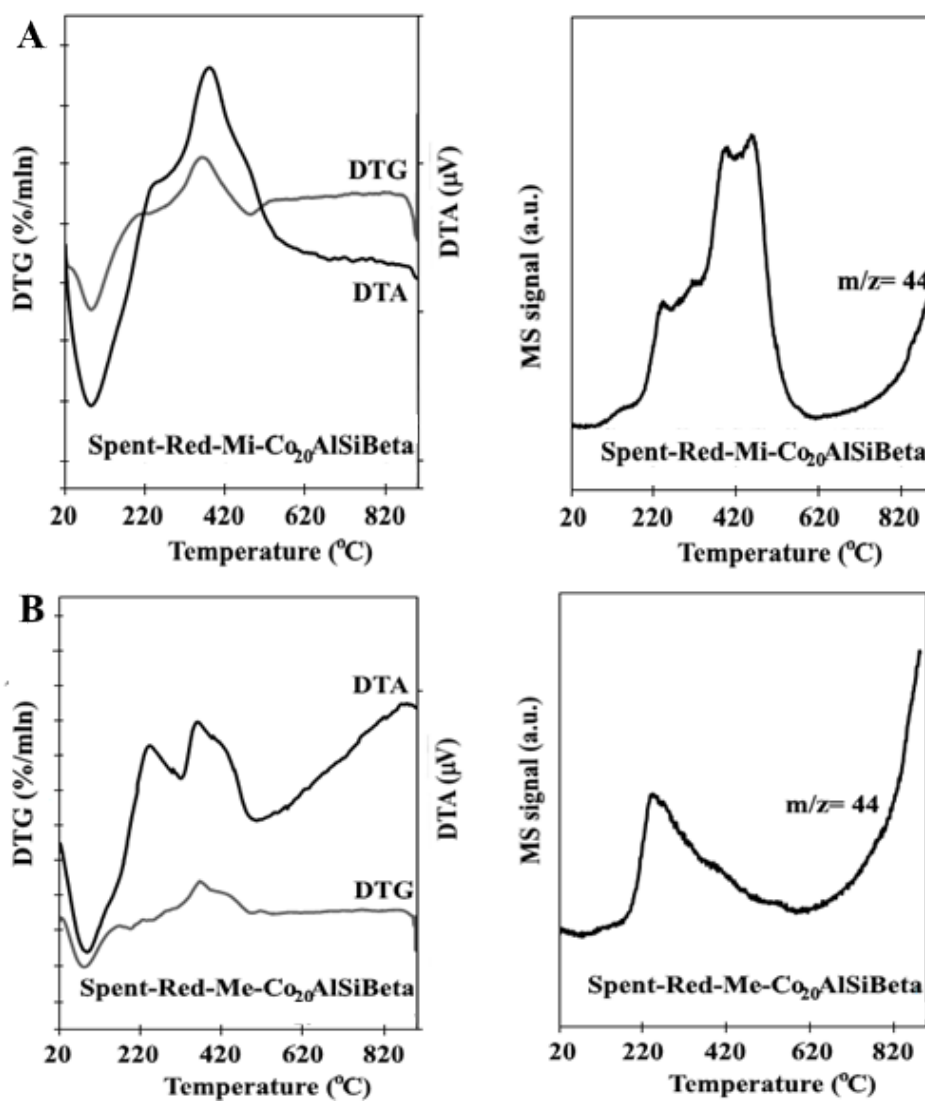


Figure 16. Investigation of carbon deposition on the (A) Spent-Red-Mi-Co<sub>20</sub>AlSiBeta and (B) Spent-Red-Me-Co<sub>20</sub>AlSiBeta.

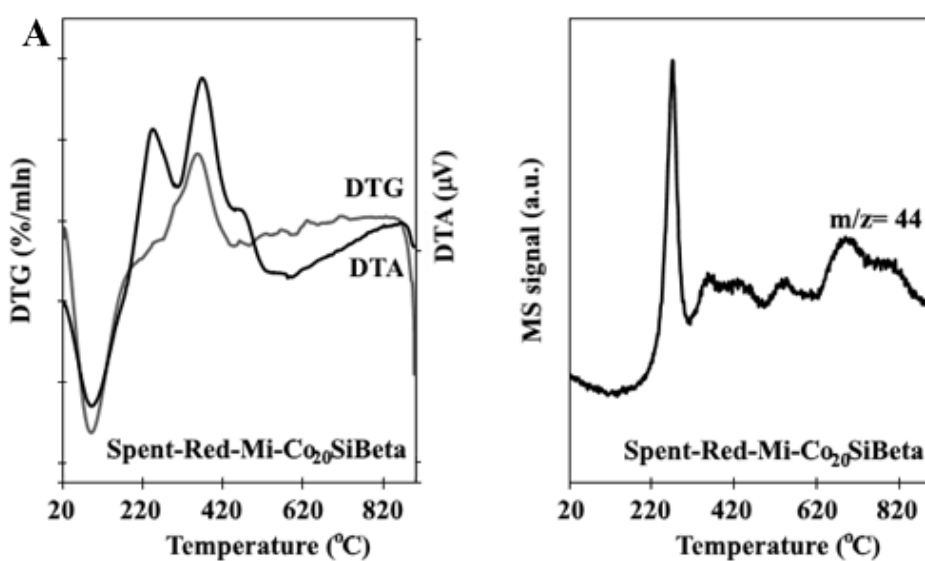
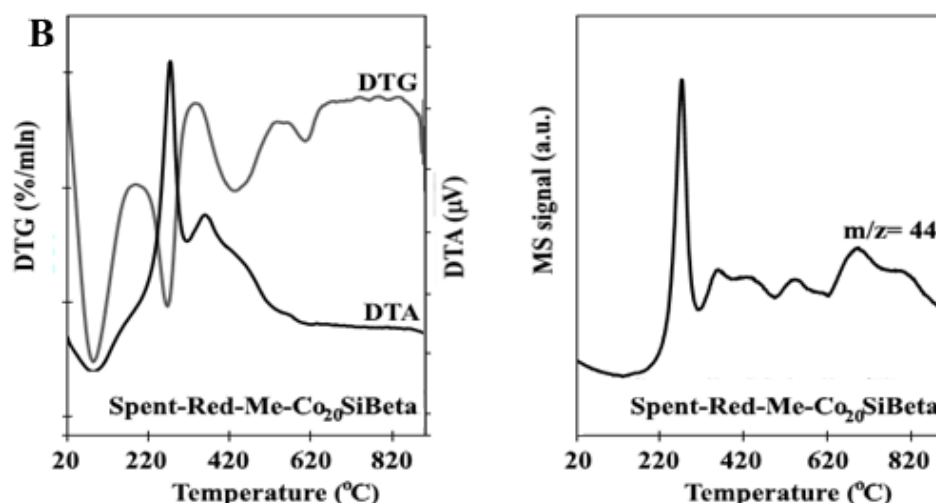


Figure 17. Cont.



**Figure 17.** Investigation of carbon deposition on the (A) Spent-Red-Mi-Co<sub>20</sub>SiBeta and (B) Spent-Red-Me-Co<sub>20</sub>SiBeta.

### 3. Materials and Methods

Two kinds of TEABeta zeolites (Si/Al = 18) with various porosity—mesoporous (Me-TEABeta) and microporous (Mi-TEABeta) were used as parent zeolite for preparation of cobalt-containing zeolite catalysts. The each parent TEABeta zeolites were divided into three parts and modified in a different way. In the Scheme 1 the consecutive steps of catalysts preparation are presented.

The first part was calcined at 550 °C for 15 h in order to obtain organic free Me-HAlBeta (Si/Al=18 (Me) (Scheme 1A) and Mi-HAlBeta (Si/Al = 18 (Mi) supports (Scheme 1B). These two supports were impregnated with the aqueous solution of Co(NO<sub>3</sub>)<sub>2</sub>·6 H<sub>2</sub>O (Sigma-Aldrich, St. Louis, MO, USA) at pH = 2.7–2.97 under stirring in aerobic conditions at room temperature for 24 h.

The second and third part of zeolite catalysts were obtained by two-step post-synthesis method which consists, in the first step, of treating of each parent Mi-TEABeta or Me-TEABeta zeolite with nitric acid with different concentration of 6 and 13 M and stirring at 80 °C for 4 h to prepare partly dealuminated HAlSiBeta support (Si/Al = 349 (Me), Si/Al = 881 (Mi)) or almost totally dealuminated support (SiBeta with (Si/Al = 490 (Me), Si/Al = 1516 (Mi)) and, in the second step, the impregnation of mesoporous and microporous HAlSiBeta or SiBeta supports with an aqueous solution of Co(NO<sub>3</sub>)<sub>2</sub> · 6 H<sub>2</sub>O at pH = 2.66–3.38 under stirring at room temperature for 24 h to obtain the solids with 20 wt% of cobalt with different Si/Al ratio.

Then, the separation of the solids from the fraction of suspension was done in evaporator under vacuum of a membrane pump for 2 h in air at 60 °C. After calcination at 500 °C for 3 h in air the obtained zeolite catalysts were labelled as Me-Co<sub>20</sub>AlBeta and Mi-Co<sub>20</sub>AlBeta for first part of zeolite catalysts and Me-Co<sub>20</sub>AlSiBeta, Me-Co<sub>20</sub>SiBeta (Scheme 1A) and Mi-Co<sub>20</sub>AlSiBeta and Mi-Co<sub>20</sub>SiBeta (Scheme 1B) for second and third part of zeolite catalysts.

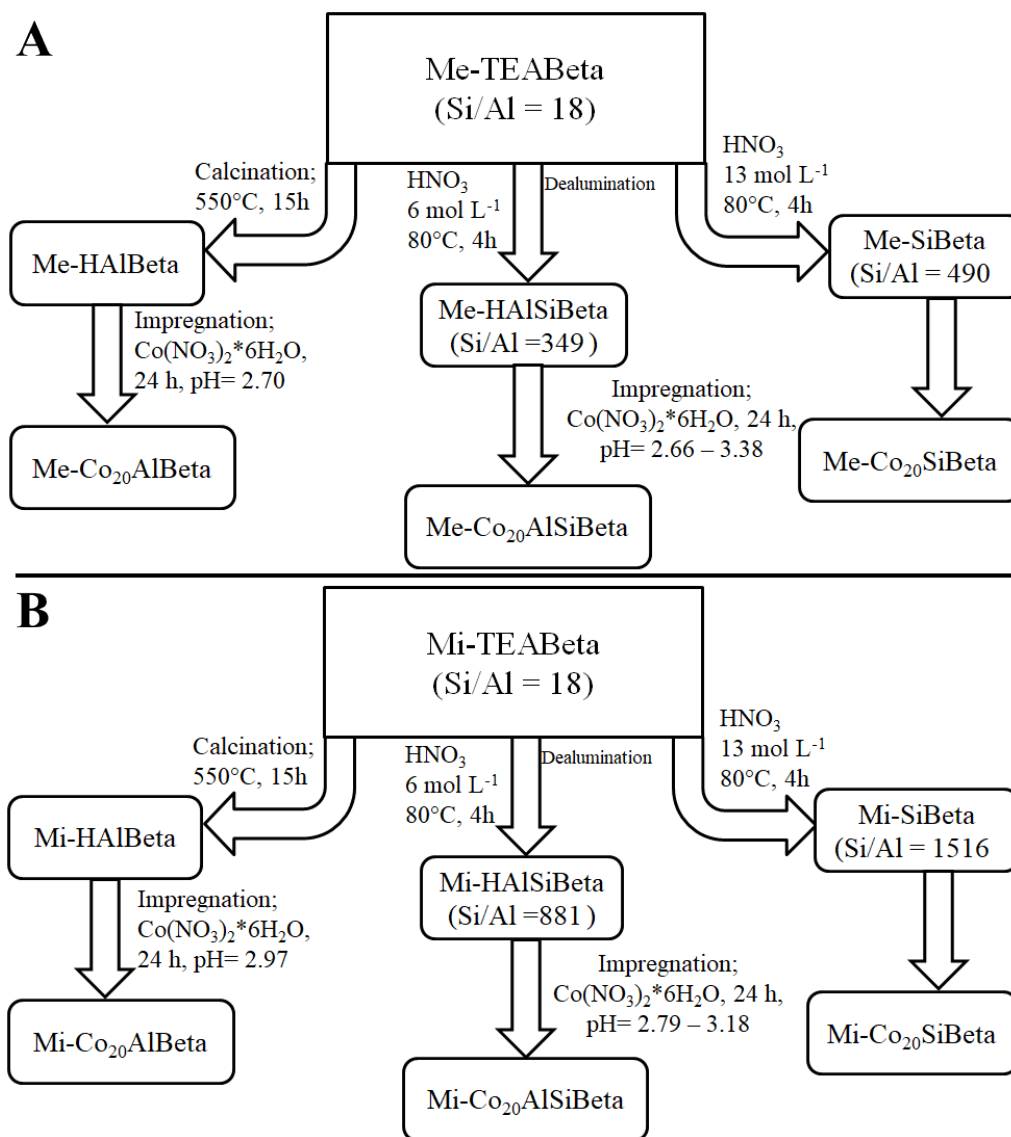
Some part of each fraction of the obtained catalytic systems was activated in situ under atmospheric pressure in the flow of the mixture 95 vol % H<sub>2</sub> and 5 vol % Ar at 400°C, which led to the formation of Red-Co<sub>20</sub>AlBeta, Red-Co<sub>20</sub>AlSiBeta and Red-Co<sub>20</sub>SiBeta.

The metal content and the Si/Al ratio of tested catalysts were obtained by chemical analysis performed on the X-ray Fluorescence (XRF) (SPECTRO X-LabPro, Kleve, Germany) at room temperature.

The XRD patterns of catalysts were obtained on PANalyticalX'Pert Pro (Malvern Panalytical Ltd., Malvern, UK) diffractometer using Cu K<sub>α</sub> radiation (λ = 154.05 pm) in 2θ range of 5–90° in ambient atmosphere.

The phase transformation of catalysts during reduction process at 300 and 400 °C was also determined. These measurements were done in situ by using the same apparatus equipped with an Anton Paar XRK900 reactor chamber. Approximately 150 mg of sample was packed in the glass ceramic

(Macor) XRD sample holder. The reagent gas used in the experiment was a mixture of 5 vol % H<sub>2</sub> and 95 vol % Ar. The sample was heated at a nominal rate of 5 °C min<sup>-1</sup>. The X-ray source was a copper long fine focus X-ray diffraction tube operating at 40 kV and 30 mA. The patterns were collected in the 2θ range of 5–80° (step 0.0167°, 50 s per step).



**Scheme 1.** Methods of preparation of (A) mesoporous and (B) microporous co-containing Beta zeolites.

The X-ray Photoelectron Spectroscopy (XPS) measurements were performed with SES R4000 hemispherical analyzer (GammadataScienta, Uppsala, Sweden). The unmonochromatized Al K $\alpha$  (1486.6 eV) X-ray source with the anode operating at 12 kV and 15 mA current emission was applied to produce core excitation. The energy resolution of the system, measured as a full width at half maximum (FWHM) for Ag 3d<sub>5/2</sub> excitation line, was 0.9 eV (pass energy 100 eV). The spectrometer was calibrated according to ISO 15472:2001. During the experiments, base pressure in the analysis chamber was about 2 × 10<sup>-9</sup> mbar. The powder samples were pressed into indium foil and installed on a dedicated holder. Detailed spectra were acquired at pass energy of 100 eV (with 25 meV step), whereas survey scans at pass energy of 200 eV (with 0.25 eV step). The sample analysis area was about 3 mm<sup>2</sup>.

Intensities were evaluated by integrating of each peak (CasaXPS 2.3.15), after subtraction of the Shirley-type background, and fitting the experimental data with a pseudo-Voigt profile of variable

proportions (70:30). The Co 2p core excitations were deconvoluted with a relative intensity ratio of 2p<sub>3/2</sub> and 2p<sub>1/2</sub> lines fixed to 2:1. All binding energy values were corrected for surface charging (C-H bonds in C 1s excitation set at 285.0 eV).

The temperature-programmed desorption of ammonia (NH<sub>3</sub>-TPD) studies were performed in a quartz reactor. Prior the measurement, the sample was pretreated at 500°C in the He flow for 30 min. Next, the reactor was cooled down to 100°C and in this temperature the adsorption of gaseous ammonia was carried out for 15 min. For removal of the physisorbed ammonia from the zeolite surface, the tested systems were flushed with helium flow at 100°C for 15 min. NH<sub>3</sub>-TPD studies were performed in the temperature range of 40–500°C. The thermal conductivity detector detected the amount of adsorbed ammonia. Additionally, in order to check the impact of metal reduction on the acidity of the sample, it was subjected to hydrogen flow at 400 °C for 1 h before performing the adsorption of gaseous ammonia.

The temperature-programmed reduction with hydrogen (TPR-H<sub>2</sub>) of cobalt-based catalysts (c.a. 0.08 g) was carried out in the U-shaped tubular quartz microreactor. The flow of reducing mixture of 5% H<sub>2</sub> in Ar was 25 mL min<sup>-1</sup> (Air Products Ltd., Poland). The measurement was performed in the temperature range of 30–900°C with the ramp rate of 10 °C min<sup>-1</sup>. The thermal conductivity detector (TCD) monitored the consumption of hydrogen (Altamira Instruments, Pittsburgh, PA, USA).

Transmission electron microscope (TEM) images were carried out using JEOL 1011 ELECTRON MICROSCOPE (JOEL, Tokyo, Japan). Before the TEM measurement, all reduced samples were ultrasonically dispersed in a pure ethanol and a drop of obtained suspension was deposited on a carbon films on copper grids.

Before the Fischer-Tropsch synthesis, all tested samples were pretreated at 400°C in the H<sub>2</sub> flow for 1 h. The reaction was performed at 30 atm and 260°C. The flow of reactant gas mixture (H<sub>2</sub>/CO = 2) was 60 mL min<sup>-1</sup>. For each measurement, 0.5 g sample was loaded in the stainless steel fix-bed flow reactor with a length of 50 cm and internal diameter of 7 mm. The bulk height of catalyst bed, placed in the middle of reactor, was 5.8 cm. The reactor was situated in furnace which length is 35 cm. The catalyst was not diluted with inert material in catalytic test. The fraction of catalyst was very fine loose powder. The stabilization of reaction conditions was carried out for 15 h. Gas products were analyzed by GC gas chromatograph (Shimadzu GC-14; Shimadzu Corporation, Duisburg, Germany) equipped with thermal conductivity detector and two columns: measuring-Carbosphere 7A and comparative-molecular sieves 7B.

Parameters of operating chromatograph:

Column temperature–45 °C

Detector temperature–120 °C

Injector temperature–120 °C

The following formulas were used to calculate the conversion of CO (K<sub>CO</sub>) and selectivity to CO<sub>2</sub> (S<sub>CO2</sub>), gaseous hydrocarbons C<sub>1</sub>-C<sub>4</sub> (S<sub>CH4</sub>), and liquid products (S<sub>LP</sub>):

$$K_{CO} = ((S_{COin} - S_{COari})/S_{COin}) \cdot 100\%$$

$$S_{CH4} = ((X_{CH4} \cdot 100\%)/X_{CH4out})/F$$

$$X_{CH4out} = (X_{CH4s} \cdot K_{CO})/100\%$$

$$S_{CO2out} = ((X_{CO2i} \cdot 100\%)/X_{CO2out})/F$$

$$X_{CO2out} = (X_{CO2s} \cdot K_{CO})/100\%$$

$$F = S_{Ar i}/S_{Ar s}$$

$$S_{LP} = 100 - (S_{CH4} + S_{CO2})$$

where:  $K_{CO}$ —Conversion of CO,  $S_{COin}$ —the area of the CO peak before reaction,  $S_{COari}$ —the area of the CO peak after reaction,  $S_{CH4}$ — $CH_4$  selectivity,  $S_{CO2}$ — $CO_2$  selectivity,  $X_{CH4i}$ —the area of the peak of obtained  $CH_4$ ,  $X_{CO2i}$ —the area of the peak of obtained  $CO_2$ ,  $X_{CH4out}$ —the area of the theoretical  $CH_4$  peak (when all CO is converted to  $CH_4$ ),  $X_{CO2out}$ —the area of the theoretical  $CO_2$  peak (when all CO is converted to  $CO_2$ ),  $X_{CH4s}$ —the area of the standard  $CH_4$  (when only  $CH_4$  is tested),  $X_{CO2s}$ —the area of the standard  $CO_2$  (when only  $CO_2$  is tested),  $F$ —contraction coefficient,  $S_{Ari}$ —the area of the Ar peak during reaction,  $S_{Ars}$ —the area of the Ar peak before reaction,  $S_{LP}$ —liquid products selectivity.

Liquid products were analyzed by GC MS (6890 N Network GC System with a Zebron Phase ZB-1MS capillary column—a length of 30 m, an internal diameter of 0.25 mm linked with a 5973 Network Mass Selective Detector mass spectrometer with a 7683 Series Injector autosampler (AGILENT, Midland, ON, Canada). The chromatographic analysis was performed in the temperature range 70–250 °C with temperature rise rate of 8 °C min<sup>-1</sup>. The initial and final temperatures were held for 3 and 30 min, respectively. The value of chain growth probability ( $\alpha$ ) was determined by using Anderson–Schultz–Floury (ASF) distribution of obtained liquid products. Assuming that  $\alpha$  is independent of the length of hydrocarbon chain, ASF equation can be represented as follows:

$$\log(W_n/n) = n \log \alpha + \text{const.}$$

where  $W_n$ —mass fraction of obtained liquid products with carbon number  $n$ . The  $\alpha$  value was calculated from the plot slope of  $\log(W_n/n)$  against  $n$ .

The carbon deposition was determined by TG-DTA-MS technique. The tests were carried out with the SETSYS 16/18 thermal analyzer from Setaram (Caluire, France) and mass spectrometer Balzers (Hiden Analytical, Düsseldorf, Germany). The measurement was carried out in the temperature range of 20–1000 °C using a linear temperature increase of 10 °C min<sup>-1</sup> and sample weight of 10 mg in dynamic conditions gas stream - Air (Air Products), the gas flow rate was 40 mL min<sup>-1</sup>. Before each measurement, the samples were outgassed in order to be purified.

#### 4. Conclusions

Two kinds of cobalt Beta zeolite catalysts (meso- and microporous) were investigated regarding their potential application in Fischer-Tropsch synthesis.

- The presence of mesopores in the zeolite structure leads to the formation of catalysts with larger Co particles, the activity of which increases with the increase of cobalt nanoparticles average size.
- In the case of mesoporous catalysts the influence of the zeolite dealumination on the catalytic performance is significant. The activity of mesoporous samples in Fischer-Tropsch synthesis increases in the following order: Red-Me-Co<sub>20</sub>AlBeta < Red-Me-Co<sub>20</sub>AlSiBeta < Red-Me-Co<sub>20</sub>SiBeta.
- For microporous catalysts the dealumination does not play such significant role and the relatively high activity is observed for both not dealuminated and dealuminated catalysts. The activity changes in the following order: Red-Mi-Co<sub>20</sub>AlSiBeta < Red-Mi-Co<sub>20</sub>AlBeta < Red-Mi-Co<sub>20</sub>SiBeta.
- The considerable difference in the activity between microporous not dealuminated (Red-Mi-Co<sub>20</sub>AlBeta) and mesoporous not dealuminated (Red-Me-Co<sub>20</sub>AlBeta) catalysts is found. The first of them shows much higher CO conversion (71%), selectivity towards liquid products (82%) and stability than the second one. This phenomenon may result from the less diversified metal nanoparticles distribution in mesopores samples.
- For both mesoporous and microporous catalysts, the main liquid products are C<sub>10</sub>-C<sub>14</sub> isoalkanes and n-alkanes. Very small amount of oxygenates (alcohols) was also identified.
- The iso-/n-alkanes ratio for catalysts supported on microporous zeolite is higher than on mesoporous one.
- The kind and amount of liquid products are related to the presence of different kind of acidic sites in dealuminated and not dealuminated zeolite catalysts.

**Author Contributions:** The experimental work was designed and supported by R.S., K.C., P.M., J.R., J.G. and S.D. The manuscript was amended and supplemented by all authors. All authors given approval for the final version of the manuscript.

**Funding:** There is not funding support for this work.

**Conflicts of Interest:** The authors declare no conflict of interest.

## References

1. Jung, J.S.; Kim, S.W.; Moon, D.J. Fischer–Tropsch Synthesis over cobalt based catalyst supported on different mesoporous silica. *Catal. Today* **2012**, *185*, 168–174. [[CrossRef](#)]
2. Najafabadi, A.T.; Khodadadi, A.A.; Parnian, M.J.; Mortazavi, Y. Atomic layer deposited Co/ $\gamma$ -Al<sub>2</sub>O<sub>3</sub> catalyst with enhanced cobalt dispersion and Fischer–Tropsch synthesis activity and selectivity. *Appl. Catal. A* **2016**, *511*, 31–46. [[CrossRef](#)]
3. Martínez, A.; López, C.; Márquez, F.; Díaz, I. Fischer–Tropsch synthesis of hydrocarbons over mesoporous Co/SBA-15 catalysts: The influence of metal loading, cobalt precursor, and promoters. *J. Catal.* **2003**, *220*, 486–499. [[CrossRef](#)]
4. Khodakov, A.Y.; Griboval-Constant, A.; Bechara, R.; Zholobenko, V.L. Pore Size Effects in Fischer Tropsch Synthesis over Cobalt-Supported Mesoporous Silicas. *J. Catal.* **2002**, *206*, 230–241. [[CrossRef](#)]
5. Xiong, H.; Zhang, Y.; Liew, K.; Li, J. Fischer–Tropsch synthesis: The role of pore size for Co/SBA-15 catalysts. *J. Mol. Catal. A Chem.* **2008**, *295*, 68–76. [[CrossRef](#)]
6. Dalil, M.; Sohrabi, M.; Royaei, S.J. Application of nano-sized cobalt on ZSM-5 zeolite as an active catalyst in Fischer–Tropsch synthesis. *J. Ind. Eng. Chem.* **2012**, *18*, 690–696. [[CrossRef](#)]
7. Subramanian, V.; Zholobenko, V.L.; Cheng, K.; Lancelot, C.; Heyte, S.; Thuriot, J.; Paul, S.; Ordonsky, V.V.; Khodakov, A.Y. The Role of Steric Effects and Acidity in the Direct Synthesis of iso-Paraffins from Syngas on Cobalt Zeolite Catalysts. *ChemCatChem* **2016**, *8*, 380–389. [[CrossRef](#)]
8. Baranak, M.; Gürünlü, B.; Sariođlan, A.; Ataç, Ö.; Atakül, H. Low acidity ZSM-5 supported iron catalysts for Fischer–Tropsch synthesis. *Catal. Today* **2013**, *207*, 57–64. [[CrossRef](#)]
9. Li, C.; Sayaka, I.; Chisato, F.; Fujimoto, K. Development of high performance graphite-supported iron catalyst for Fischer–Tropsch synthesis. *Appl. Catal. A* **2016**, *509*, 123–129. [[CrossRef](#)]
10. Wang, S.; Yin, Q.; Guo, J.; Ru, B.; Zhu, L. Improved Fischer–Tropsch synthesis for gasoline over Ru, Ni promoted Co/HZSM-5 catalysts. *Fuel* **2013**, *108*, 597–603. [[CrossRef](#)]
11. Jahangiri, H.; Bennett, J.; Mahjoubi, P.; Wilson, K.; Gu, S. A review of advanced catalyst development for Fischer–Tropsch synthesis of hydrocarbons from biomass derived syn-gas. *Catal. Sci. Technol.* **2014**, *4*, 2210–2229. [[CrossRef](#)]
12. Kang, S.-H.; Ryu, J.-H.; Kim, J.-H.; Prasad, P.S.S.; Bae, J.W.; Cheon, J.-Y.; Jun, K.-W. ZSM-5 Supported Cobalt Catalyst for the Direct Production of Gasoline Range Hydrocarbons by Fischer–Tropsch Synthesis. *Catal. Lett.* **2011**, *141*, 1464–1471. [[CrossRef](#)]
13. Wang, Y.; Jiang, Y.; Huang, J.; Liang, J.; Wang, H.; Li, Z.; Wu, J.; Li, M.; Zhao, Y.; Niu, J. Effect of hierarchical crystal structures on the properties of cobalt catalysts for Fischer–Tropsch synthesis. *Fuel* **2016**, *174*, 17–24. [[CrossRef](#)]
14. Xing, C.; Yang, G.; Wu, M.; Yang, R.; Tan, L.; Zhu, P.; Wei, Q.; Li, J.; Mao, J.; Yoneyama, Y.; et al. Hierarchical zeolite Y supported cobalt bifunctional catalyst for facilely tuning the product distribution of Fischer–Tropsch synthesis. *Fuel* **2015**, *148*, 48–57. [[CrossRef](#)]
15. Botes, F.G.; Böhringer, W. The addition of HZSM-5 to the Fischer–Tropsch process for improved gasoline production. *Appl. Catal. A* **2004**, *267*, 217–225. [[CrossRef](#)]
16. Chalupka, K.A.; Casale, S.; Zurawicz, E.; Rynkowski, J.; Dzwigaj, S. The remarkable effect of the preparation procedure on the catalytic activity of CoBEA zeolites in the Fischer–Tropsch synthesis. *Microporous Mesoporous Mater.* **2015**, *211*, 9–18. [[CrossRef](#)]
17. Concepción, P.; López, C.; Martínez, A.; Puentes, V.F. Characterization and catalytic properties of cobalt supported on delaminated ITQ-6 and ITQ-2 zeolites for the Fischer–Tropsch synthesis reaction. *J. Catal.* **2004**, *228*, 321–332. [[CrossRef](#)]

18. Prieto, G.; Martínez, A.; Concepción, P.; Moreno-Tost, R. Cobalt particle size effects in Fischer–Tropsch synthesis: Structural and in situ spectroscopic characterisation on reverse micelle-synthesised Co/ITQ-2 model catalysts. *J. Catal.* **2009**, *266*, 129–144. [CrossRef]
19. Newsam, J.M.; Treacy, M.M.J.; Koetsier, W.T.; Gruyter, C.B. Structural characterization of zeolite beta. *Proc. R. Soc. Lond. Ser. A* **1988**, *420*, 375–405. [CrossRef]
20. Dzwigaj, S.; Janas, J.; Machej, T.; Che, M. Selective catalytic reduction of NO by alcohols on Co- and Fe-Si $\beta$  catalysts. *Catal. Today* **2007**, *119*, 133–136. [CrossRef]
21. Dzwigaj, S.; Millot, Y.; Méthivier, C.; Che, M. Incorporation of Nb(V) into BEA zeolite investigated by XRD, NMR, IR, DR UV–vis, and XPS. *Microporous Mesoporous Mater.* **2010**, *130*, 162–166. [CrossRef]
22. Wang, H.; Li, B.; Lu, X.-B.; Li, C.-Q.; Ding, F.-C.; Song, Y.-J. Selective catalytic reduction of NO by methane over the Co/MOR catalysts in the presence of oxygen. *J. Fuel Chem. Technol.* **2015**, *43*, 1106–1112. [CrossRef]
23. Shi, L.; Tao, K.; Kawabata, T.; Shimamura, T.; Zhang, X.J.; Tsubaki, N. Surface Impregnation Combustion Method to Prepare Nanostructured Metallic Catalysts without Further Reduction: As-Burnt Co/SiO $_2$  Catalysts for Fischer–Tropsch Synthesis. *ACS Catal.* **2011**, *1*, 1225–1233. [CrossRef]
24. Khemtong, P.; Klysubun, W.; Prayoonpokarach, S.; Wittayakun, J. Reducibility of cobalt species impregnated on NaY and HY zeolites. *Mater. Chem. Phys.* **2010**, *121*, 131–137. [CrossRef]
25. Khodakov, A.Y.; Lynch, J.; Bazin, D.; Rebours, B.; Zanier, N.; Moisson, B.; Chaumette, P. Reducibility of Cobalt Species in Silica-Supported Fischer–Tropsch Catalysts. *J. Catal.* **1997**, *168*, 16–25. [CrossRef]
26. Kumar, M.S.; Schwidder, M.; Grünert, W.; Bentrup, U.; Brückner, A. Selective reduction of NO with Fe-ZSM-5 catalysts of low Fe content: Part II. Assessing the function of different Fe sites by spectroscopic in situ studies. *J. Catal.* **2006**, *239*, 173–186.
27. Arishtirova, K.; Kovacheva, P.; Predoeva, A. Activity and basicity of BaO modified zeolite and zeolite-type catalysts. *Appl. Catal. A* **2003**, *243*, 191–196. [CrossRef]
28. Kovacheva, P.; Arishtirova, K.; Predoeva, A. Basic zeolite and zeolite-type catalysts for the oxidative methylation of toluene with methane. *React. Kinet. Catal. Lett.* **2003**, *79*, 149–155. [CrossRef]
29. Oleksenko, L.P. Characteristics of Active Site Formation in Co-Containing Catalysts for CO Oxidation on Chemically Different Supports. *Theor. Exp. Chem.* **2004**, *40*, 331–336. [CrossRef]
30. Grünert, W.; Schlögl, R. Photoelectron Spectroscopy of Zeolites. *Mol. Sieves* **2004**, *4*, 467–515.
31. Kocemba, I.; Rynkowski, J.; Gurgul, J.; Socha, R.P.; Łatka, K.; Krafft, J.-M.; Dzwigaj, S. Nature of the active sites in CO oxidation on FeSiBEA zeolites. *Appl. Catal. A* **2016**, *519*, 16–26. [CrossRef]
32. Boroń, P.; Chmielarz, L.; Gurgul, J.; Łatka, K.; Gil, B.; Marszałek, B.; Dzwigaj, S. Influence of iron state and acidity of zeolites on the catalytic activity of FeHBEA, FeHZSM-5 and FeHMOR in SCR of NO with NH $_3$  and N $_2$ O decomposition. *Microporous Mesoporous Mater.* **2015**, *203*, 73–85. [CrossRef]
33. Janas, J.; Gurgul, J.; Socha, R.P.; Dzwigaj, S. Effect of Cu content on the catalytic activity of CuSiBEA zeolite in the SCR of NO by ethanol: Nature of the copper species. *Appl. Catal. B* **2009**, *91*, 217–224. [CrossRef]
34. Boroń, P.; Chmielarz, L.; Gurgul, J.; Łatka, K.; Shishido, T.; Krafft, J.-M.; Dzwigaj, S. BEA zeolite modified with iron as effective catalyst for N $_2$ O decomposition and selective reduction of NO with ammonia. *Appl. Catal. B* **2013**, *138–139*, 434–445. [CrossRef]
35. NIST X-ray Photoelectron Spectroscopy Database. Available online: <http://srdata.nist.gov/xps/> (accessed on 13 September 2018).
36. Chen, H.-H.; Shen, S.-C.; Chen, X.; Kawi, S. Selective catalytic reduction of NO over Co/beta-zeolite: Effects of synthesis condition of beta-zeolites, Co precursor, Co loading method and reductant. *Appl. Catal. B* **2004**, *50*, 37–47. [CrossRef]
37. Zsoldos, Z.; Vass, G.; Lu, G.; Gucci, L. XPS study on the effects of treatments on Pt $^{2+}$  and Co $^{2+}$  exchanged into NaY zeolite. *Appl. Surf. Sci.* **1994**, *78*, 467–475. [CrossRef]
38. Boix, A.V.; Zamaro, J.M.; Lombardo, E.A.; Miro, E.E. The beneficial effect of silica on the activity and thermal stability of PtCoFerrierite-washcoated cordierite monoliths for the SCR of NO $_x$  with CH $_4$ . *Appl. Catal. B* **2003**, *46*, 121–132. [CrossRef]
39. Da Cruz, R.S.; Mascarenhas, A.J.S.; Andrade, H.M.C. Co-ZSM-5 catalysts for N $_2$ O decomposition. *Appl. Catal. B* **1998**, *18*, 223–231. [CrossRef]
40. Stencel, J.M.; Rao, V.U.S.; Diehl, J.R.; Rhee, K.H.; Dhere, A.G.; De Angelis, R.J. Dual cobalt speciation in CoZSM-5 catalysts. *J. Catal.* **1983**, *84*, 109–118. [CrossRef]

41. Dzwigaj, S.; Janas, J.; Mizera, J.; Gurgul, J.; Socha, R.P.; Che, M. Incorporation of Copper in SiBEA Zeolite as Isolated Lattice Mononuclear Cu(II) Species and its Role in Selective Catalytic Reduction of NO by Ethanol. *Catal. Lett.* **2008**, *126*, 36–42. [[CrossRef](#)]
42. Janas, J.; Gurgul, J.; Socha, R.P.; Shishido, T.; Che, M.; Dzwigaj, S. Selective catalytic reduction of NO by ethanol: Speciation of iron and “structure–properties” relationship in FeSiBEA zeolite. *Appl. Catal. B* **2009**, *91*, 113–122. [[CrossRef](#)]
43. Janas, J.; Gurgul, J.; Socha, R.P.; Kowalska, J.; Nowinska, K.; Shishido, T.; Che, M.; Dzwigaj, S. Influence of the Content and Environment of Chromium in CrSiBEA Zeolites on the Oxidative Dehydrogenation of Propane. *J. Phys. Chem. C* **2009**, *113*, 13273–13281. [[CrossRef](#)]
44. Sartipi, S.; Parashar, K.; Valero-Romero, M.J.; Santos, V.P.; van der Linden, B.; Makkee, M.; Kapteijn, F.; Gascon, J. Hierarchical H-ZSM-5-supported cobalt for the direct synthesis of gasoline-range hydrocarbons from syngas: Advantages, limitations, and mechanistic insight. *J. Catal.* **2013**, *305*, 179–190. [[CrossRef](#)]
45. Boroń, P.; Chmielarz, L.; Casal, S.; Calers, C.; Krafft, J.-M.; Dzwigaj, S. Effect of Co content on the catalytic activity of CoSiBEA zeolites in N<sub>2</sub>O decomposition and SCR of NO with ammonia. *Catal. Today* **2015**, *258*, 507–517. [[CrossRef](#)]
46. Karimi, S.; Tavasoli, A.; Mortazavi, Y.; Karimi, A. Enhancement of cobalt catalyst stability in Fischer–Tropsch synthesis using graphene nanosheets as catalyst support. *Chem. Eng. Res. Des.* **2015**, *104*, 713–722. [[CrossRef](#)]
47. Tavasoli, A.; Malek Abbaslou, R.M.; Dalai, A.K. Deactivation behavior of ruthenium promoted Co/ $\gamma$ -Al<sub>2</sub>O<sub>3</sub> catalysts in Fischer–Tropsch synthesis. *Appl. Catal. A* **2008**, *346*, 58–64. [[CrossRef](#)]
48. Sartipi, S.; Parashar, K.; Makkee, M.; Gascon, J.; Kapteijn, F. Breaking the Fischer–Tropsch synthesis selectivity: Direct conversion of syngas to gasoline over hierarchical Co/H-ZSM-5 catalysts. *Catal. Sci. Technol.* **2013**, *3*, 572–575. [[CrossRef](#)]
49. Martinez, A.; Lopez, C. The influence of ZSM-5 zeolite composition and crystal size on the in situ conversion of Fischer–Tropsch products over hybrid catalysts. *Appl. Catal. A* **2005**, *294*, 251–259. [[CrossRef](#)]
50. Peña, D.; Griboval-Constant, A.; Lancelot, C.; Quijada, M.; Visez, N.; Stéphan, O.; Lecocq, V.; Diehl, F.; Khodakov, A.Y. Molecular structure and localization of carbon species in alumina supported cobalt Fischer–Tropsch catalysts in a slurry reactor. *Catal. Today* **2014**, *228*, 65–76. [[CrossRef](#)]
51. Moodley, D.J.; van de Loosdrecht, J.; Saib, A.M.; Overett, M.J.; Datye, A.K.; Niemantsverdriet, J.W. Carbon deposition as a deactivation mechanism of cobalt-based Fischer–Tropsch synthesis catalysts under realistic conditions. *Appl. Catal. A Gen.* **2009**, *354*, 102–110. [[CrossRef](#)]
52. Bartholomew, C.H.; Farrauto, R.J. *Fundamentals of Industrial Catalytic Processes*, 2nd ed.; Chapter 5; Wiley Interscience: New York, NY, USA, 2010; pp. 260–336.



© 2019 by the authors. Licensee MDPI, Basel, Switzerland. This article is an open access article distributed under the terms and conditions of the Creative Commons Attribution (CC BY) license (<http://creativecommons.org/licenses/by/4.0/>).